Defective fatty acid oxidation in mice with muscle-specific acyl-CoA synthetase 1 deficiency increases amino acid use and impairs muscle function

Received for publication, November 20, 2018, and in revised form, March 21, 2019 Published, Papers in Press, April 11, 2019, DOI 10.1074/jbc.RA118.006790

Liyang Zhao[‡], Florencia Pascual[‡], Lawrence Bacudio[‡], Amanda L. Suchanek[‡], Pamela A. Young[‡], Lei O. Li[‡], Sarah A. Martin[§], Joao-Paulo Camporez[¶], Rachel J. Perry[¶‖], Gerald I. Shulman[¶‖], Eric L. Klett[**], and Rosalind A. Coleman[‡1]

From the Departments of [‡]Nutrition and [**]Medicine, University of North Carolina, Chapel Hill, North Carolina 27599, the [§]Department of Molecular Genetics and Internal Medicine, University of Texas Southwestern Medical Center, Dallas, Texas 75390, and the Departments of [¶]Internal Medicine and [‖]Cellular and Molecular Physiology, Yale University School of Medicine, New Haven, Connecticut 06520

Edited by George M. Carman

Loss of long-chain acyl-CoA synthetase isoform-1 (ACSL1) in mouse skeletal muscle ($Acsl1^{M-/-}$) severely reduces acyl-CoA synthetase activity and fatty acid oxidation. However, the effects of decreased fatty acid oxidation on skeletal muscle function, histology, use of alternative fuels, and mitochondrial function and morphology are unclear. We observed that $Acsl1^{M-/-}$ mice have impaired voluntary running capacity and muscle grip strength and that their gastrocnemius muscle contains myocytes with central nuclei, indicating muscle regeneration. We also found that plasma creatine kinase and aspartate aminotransferase levels in $Acsl1^{M-/-}$ mice are 3.4- and 1.5-fold greater, respectively, than in control mice ($Acsl1^{flox/flox}$), indicating muscle damage, even without exercise, in the $Acsl1^{M-/-}$ mice. Moreover, caspase-3 protein expression exclusively in $Acsl1^{M-/-}$ skeletal muscle and the presence of cleaved caspase-3 suggested myocyte apoptosis. Mitochondria in $Acsl1^{M-/-}$ skeletal muscle were swollen with abnormal cristae, and mitochondrial biogenesis was increased. Glucose uptake did not increase in $Acsl1^{M-/-}$ skeletal muscle, and pyruvate oxidation was similar in gastrocnemius homogenates from $Acsl1^{M-/-}$ and control mice. The rate of protein synthesis in $Acsl1^{M-/-}$ glycolytic muscle was 2.1-fold greater 30 min after exercise than in the controls, suggesting resynthesis of proteins catabolized for fuel during the exercise. At this time, mTOR complex 1 was activated, and autophagy was blocked. These results suggest that fatty acid oxidation is critical for normal skeletal muscle homeostasis during both rest and exercise. We conclude that ACSL1 deficiency produces an overall defect in muscle fuel metabolism that increases protein catabolism, resulting in exercise intolerance, muscle weakness, and myocyte apoptosis.

The ability to switch between fatty acid oxidation (FAO)[2] and glycolysis is a well-studied feature of muscle metabolism (1), but it is not known whether FAO is absolutely essential for muscle homeostasis. Skeletal muscle exhibits plasticity and complexity in its choice of fuel substrate. Glycolytic fibers, such as white gastrocnemius, contain fewer mitochondria and rely more on glycolysis to generate ATP than do oxidative fibers, such as red gastrocnemius and soleus, which prefer oxidative phosphorylation (2). During starvation, fatty acids are the major fuel source, and released gluconeogenic amino acids are taken up by the liver and used for gluconeogenesis. Fatty acids are preferentially used during both rest and prolonged exercise, but during acute, intense exercise, muscle switches to glycogen and plasma glucose as its primary fuel (3, 4). The inability of skeletal muscle to use fatty acids for energy results in fatigue, exercise intolerance, and muscle weakness (5–10). These symptoms are present in genetic deficiencies of medium chain acyl-CoA dehydrogenase (*ACADM*), very long chain acyl-CoA dehydrogenase (*ACADVL*), and carnitine palmitoyltransferase 2 (*CPT2*), but the mechanisms by which reduced FAO causes muscle injury are poorly understood. Defects in FAO might restrict fuel availability, alter membrane phospholipid composition, or increase the presence of toxic metabolites. Indeed, lipid metabolism plays multifaceted roles in maintaining normal muscle physiology and function (11).

For long-chain fatty acids to be oxidized, they must first be activated to form acyl-CoAs by a member of the family of long-chain acyl-CoA synthetases (ACSL) (12). In highly oxidative tissues, such as heart, brown adipose, and skeletal muscle, acyl-CoAs destined for FAO are synthesized by ACSL1 (13–16).

This work was supported by National Institutes of Health Grants DK59935 and DK56598 (to R. A. C.), DK107481 (to E. L. K.), CA-215315 (to R. J. P.), and DK116774 and DK045735 (to G. I. S.). The authors declare that they have no conflicts of interest with the contents of this article. The content is solely the responsibility of the authors and does not necessarily represent the official views of the National Institutes of Health.
This article contains Table S1 and Figs. S1–S9.

[1] To whom correspondence should be addressed: 2301 Michael Hooker Research Center, Dauer Dr., Dept. of Nutrition, University of North Carolina, Chapel Hill, NC 27599. E-mail: rcoleman@unc.edu.

[2] The abbreviations used are: FAO, fatty acid oxidation; ACS, acyl-CoA synthetase; ACSL, long-chain ACS(s); CL, cardiolipin; CPT, carnitine palmitoyltransferase; IP, intraperitoneally; OCR, O_2 consumption rate; ORO, Oil Red O staining; PC, phosphatidylcholine; PE, phosphatidylethanolamine; SDH, succinate dehydrogenase; TAG, triacylglycerol; IL, interleukin; BCAA, branched-chain amino acid; BCKDH, branched-chain α-keto acid dehydrogenase complex; VLCAD, very-long-chain acyl-CoA dehydrogenase; PA, phosphatidic acid; PI, phosphatidylinositol; PG, phosphatidylglycerol; PS, phosphatidylserine; mTOR, mechanistic target of rapamycin; FCCP, carbonyl cyanide-4-(trifluoromethoxy)-phenylhydrazone; GAPDH, glyceraldehyde-3-phosphate dehydrogenase.

© 2019 Zhao et al. Published under exclusive license by The American Society for Biochemistry and Molecular Biology, Inc.

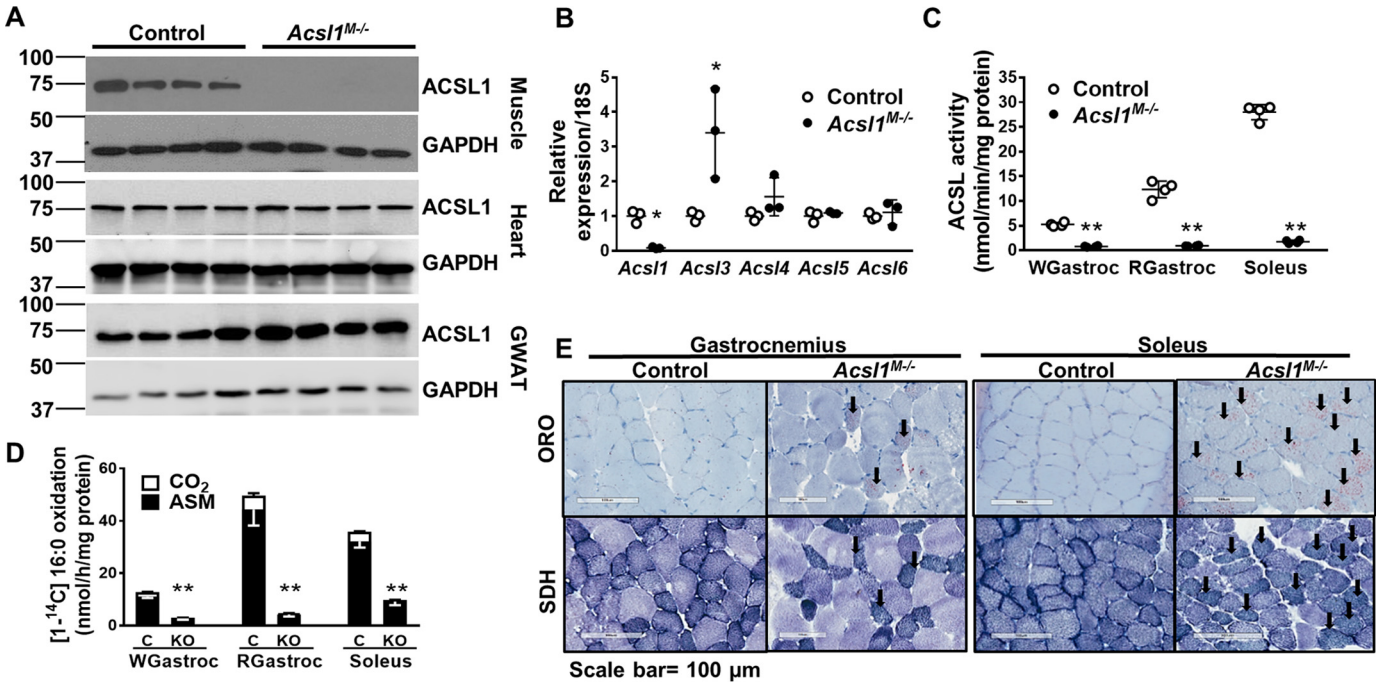

Figure 1. Lack of ACSL1 reduced muscle ACSL activity and FAO. *A*, homogenates of gastrocnemius, heart, and gonadal white adipose tissue (*GWAT*) were subjected to Western blotting and probed with anti-ACSL1 and anti-GAPDH antibodies. *B*, mRNA expression of *Acsl* isoforms in soleus. Data were normalized to 18S mRNA, $n = 3$ per genotype. *C*, ACS-specific activity of total membrane preparations from white gastrocnemius (*WGastroc*), red gastrocnemius (*RGastroc*), and soleus, $n = 4$ per genotype. *D*, [1-^{14}C]palmitate oxidation in homogenates from white gastrocnemius, red gastrocnemius, and soleus. *C*, control. *KO*, $Acsl1^{M-/-}$, $n = 3$–4 per genotype. *E*, muscles were snap-frozen in liquid nitrogen–cooled isopentane, and adjacent sections were stained with ORO or SDH. Shown are representative 100-μm images of ORO- and SDH-stained sections from gastrocnemius and soleus. Data are presented as means ± S.D. (*error bars*). **, $p < 0.01$; *, $p < 0.05$.

Deficiency of ACSL1 in the heart, for example, results in a 95% reduction in FAO and an 8-fold increase in glucose uptake, and the activation of mTORC1 contributes to cardiac hypertrophy (15, 17). Similarly, FAO is 90% lower in mice lacking ACSL1 in skeletal muscle ($Acsl1^{M-/-}$) than in littermate controls, but severe hypoglycemia also occurs and prevents $Acsl1^{M-/-}$ mice from sustaining exercise (16). Additionally, $Acsl1^{M-/-}$ deficiency causes muscle damage, as evidenced by myocytes with central nuclei and by elevated plasma creatine kinase (16). We hypothesized that defective FAO in $Acsl1^{M-/-}$ skeletal muscle would increase the use of glucose and amino acids for energy during both rest and exercise. However, our data reveal that unlike *Acsl1* deficiency in the heart, deletion of skeletal muscle *Acsl1* did not increase glucose uptake, but instead, produced a drain on muscle amino acids both during the exercise itself and after exercise when protein synthesis was enhanced. In addition, the inability to use fatty acids as a fuel substrate also increased mitochondrial biogenesis, disordered mitochondrial morphology, and increased myofiber regeneration. Surprisingly, muscle damage was more pronounced in glycolytic than in oxidative fibers.

Results

Fatty acid use was reduced in skeletal muscle from $Acsl1^{M-/-}$ mice

ACSL1 protein was absent in gastrocnemius but present in heart and gonadal white adipose tissue (*GWAT*), confirming the specificity of the skeletal muscle knockout (Fig. 1*A*). Compared with controls, *Acsl3* mRNA was 3.4-fold greater in $Acsl1^{M-/-}$ soleus (Fig. 1*B*). We previously reported greater *Acsl3* mRNA (1.5-fold) in $Acsl1^{M-/-}$ gastrocnemius than in controls (16), as well as up-regulation of *Acsl3* in ACSL1-deficient heart (16, 18). However, despite the increase in *Acsl3* mRNA, total acyl-CoA synthetase (ACS) activity was almost 90% less in both glycolytic (white gastrocnemius) and oxidative muscles (red gastrocnemius and soleus) from $Acsl1^{M-/-}$ mice, indicating minimal compensation of enzyme activity by ACSL3 (Fig. 1*C*). Similarly, loss of ACSL1 reduced the rate of FAO by 90, 77, and 72% in red and white gastrocnemius and soleus, respectively. The reduction in FAO was more pronounced in gastrocnemius, a mixed muscle, than in soleus, which contains primarily oxidative fibers (Fig. 1, *D* and *E*).

Despite reduced FAO, muscle use of glucose did not increase

ORO and SDH staining showed that in $Acsl1^{M-/-}$ mice, lipid droplets were more prominent in soleus than in gastrocnemius (Fig. 1*E*). Consistent with the histology, triacylglycerol (TAG) content increased 2.5-fold in soleus (Fig. 2*A*). Because FAO is 72–90% lower in $Acsl1^{M-/-}$ skeletal muscle than in controls, we hypothesized that glucose use would increase to compensate for the deficiency in FAO, as occurs in hearts lacking ACSL1 (15). Supporting this hypothesis, although glycogen content was unchanged in glycolytic white gastrocnemius under fed conditions, the glycogen content of both red gastrocnemius and soleus in $Acsl1^{M-/-}$ mice was ~50% lower than controls (Fig. 2*B*), suggesting enhanced glycogen use in $Acsl1^{M-/-}$ oxidative muscle. Because reduced glycogen content can result from either increased glucose use or reduced

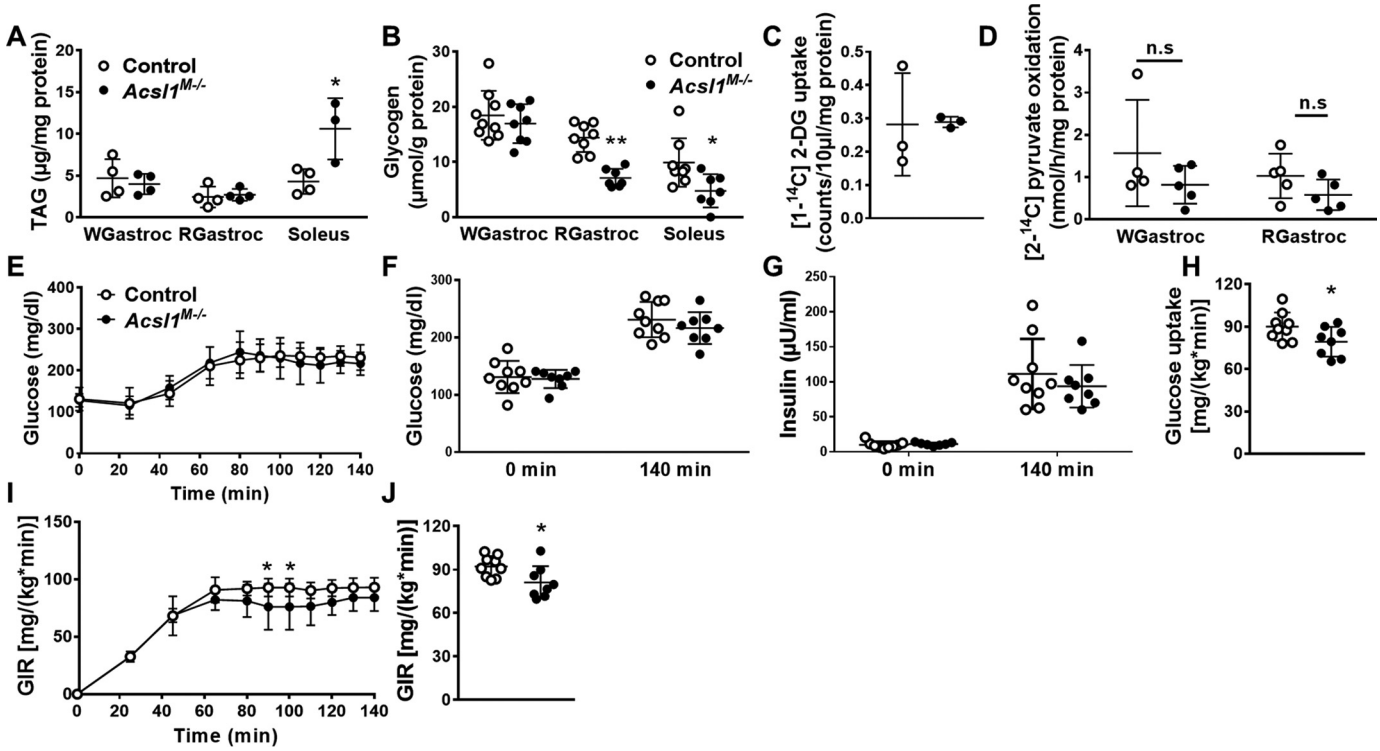

Figure 2. Lack of ACSL1 decreased muscle glycogen content, but glucose use was unchanged. *A*, TAG content of white gastrocnemius (*WGastroc*), red gastrocnemius (*RGastroc*), and soleus, $n = 3–4$ per genotype. *B*, glycogen content of white gastrocnemius, red gastrocnemius, and soleus in unfasted mice at 10 a.m. to 11 a.m., $n = 7–9$ per genotype. *C*, 2-[1-^{14}C]deoxyglucose uptake in gastrocnemius in mice deprived of food for 3 h and then exposed to 4 °C for 2 h, $n = 3$ per genotype. *D*, [2-^{14}C]pyruvate oxidation in white and red gastrocnemius homogenates, $n = 4–5$ per genotype. *E–J*, hyperinsulinemic-hyperglycemic clamp study, $n = 8–9$ per genotype; *E*, glucose was clamped at 225 mg/dl; *F*, glucose concentrations at 0 and 140 min (clamped). *G*, insulin concentration at 0 and 140 min (clamped); *H*, whole-body glucose uptake. *I*, glucose infusion rate. *J*, area under curve for glucose infusion rate. Data are presented as means ± S.D. (*error bars*). **, $p < 0.01$; *, $p < 0.05$.

glycogen synthesis, we measured the uptake of 2-[1-^{14}C]deoxyglucose during shivering thermogenesis, which promotes muscle glucose uptake (19). Mice were kept at 4 °C for 2 h, and glucose uptake was measured while mice were shivering. Surprisingly, despite muscle activity, skeletal muscle glucose uptake was similar in control and $Acsl1^{M-/-}$ gastrocnemius (Fig. 2*C*). Consistent with the lack of enhanced glucose uptake, [2-^{14}C]pyruvate oxidation did not differ between genotypes (Fig. 2*D*). Similarly, mRNA expression of pyruvate dehydrogenase subunit I (*Pdha1*) and citrate synthase (*Cs*) did not change (Fig. S1). A hyperinsulinemic-hyperglycemic clamp with glucose clamped at ~225 mg/dl (Fig. 2, *E–G*) showed lower whole-body glucose uptake and a slightly lower glucose infusion rate in $Acsl1^{M-/-}$ mice than in controls (Fig. 2, *H–J*). These data indicate that even when surplus glucose and insulin were provided, glucose uptake was mildly reduced in $Acsl1^{M-/-}$ mice. Taken as a whole, these data indicate that, in marked contrast to ACSL1-deficient heart, which also had a 90% decrease in FAO and manifested an ~8-fold increase in insulin-stimulated glucose uptake, the inability to activate long-chain fatty acids for oxidation in skeletal muscle did not increase glucose use in ACSL1-deficient muscle.

Loss of ACSL impaired voluntary running capacity and muscle grip strength

During both low-intensity and prolonged exercise, skeletal muscle primarily oxidizes fatty acid to generate ATP (20). We previously reported that endurance exercise capacity is impaired in $Acsl1^{M-/-}$ mice because of severe hypoglycemia (16). To determine whether the reduction in FAO would alter voluntary running capacity, $Acsl1^{M-/-}$ mice were allowed access to running wheels for 2 weeks. Compared with controls, $Acsl1^{M-/-}$ mice ran 21% less in total distance (Fig. 3*A*), and their average and maximal running speeds were slower during the dark cycle, when mice are the most active (Fig. 3, *B* and *C*). Moreover, the lack of ACSL1 also resulted in longer break times (times during the dark cycle in which the mice did not run) on days 2 and 3 (Fig. 3*D*), although no genotype difference was observed when total nonrunning times were calculated for the 2-week period (Fig. 3*E*). No differences between genotypes were detected in average speed, maximal speed, or break intervals during the light period (Fig. S2, *A–C*). In addition to the impairments in exercise capacity, the wire hang grip test indicated that $Acsl1^{M-/-}$ mice had severely diminished overall muscle strength (Fig. 3*F*).

Characterization of $Acsl1^{M-/-}$ myopathy

In muscle, carnitine palmitoyltransferase (CPT)-1b directs the entry of long chain acyl-CoAs from cytosol into the mitochondrial matrix to initiate β-oxidation. Mice lacking muscle CPT1b ($Cpt1b^{M-/-}$) develop myodegeneration, impaired endurance during treadmill exercise, and gait disturbances at 1 year of age (21). Muscle-specific CPT1b deficiency inhibits mitochondrial FAO, promotes mitochondrial biogenesis, and

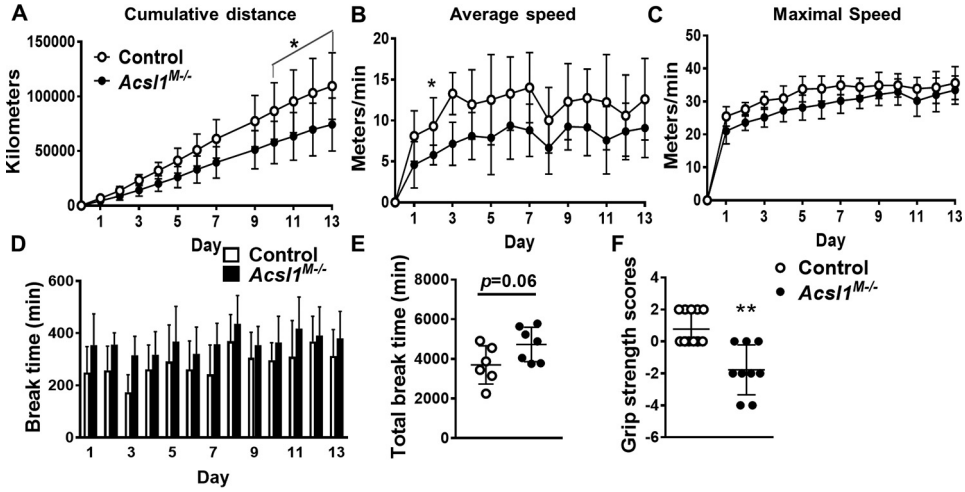

Figure 3. Voluntary running capacity was impaired in $Acsl1^{M-/-}$ mice. *A–E*, mice were individually housed for 2 weeks with access to a running wheel in a room with a 12-h light/dark cycle, $n = 6–7$ per genotype. *A*, cumulative distance run. *B*, daily average running speed during the dark period. *C*, daily maximal running speed during the dark period. *D*, approximate length of time during which mice did not run during the dark period. *E*, sum of each day's break time. *F*, grip strength in control and $Acsl1^{M-/-}$ mice, $n = 9–11$ per genotype. Data are presented as means ± S.D. (*error bars*). **, $p < 0.01$; *, $p < 0.05$.

induces compensatory peroxisomal FAO and amino acid oxidation (21). Because skeletal muscle ACSL1 is required to synthesize the acyl-CoAs used by CPT1b (22), we asked whether loss of ACSL1 would also result in muscle damage. Compared with control mice, biomarkers of skeletal muscle damage, serum creatine kinase and aspartate transaminase levels, were 3.5- and 1.5-fold greater, respectively (Fig. 4, *A* and *B*). Unlike cardiac muscle, damaged skeletal muscle can regenerate, and regeneration is manifested by the presence of central nuclei (23). Although $Acsl1^{M-/-}$ skeletal muscle showed no signs of necrosis (Fig. S3), in unexercised mice, 8.3% of $Acsl1^{M-/-}$ gastrocnemius cells contained central nuclei, compared with only 0.8% of cells in control gastrocnemius (Fig. 4, *C* and *E*). After voluntary exercise on running wheels for 2 weeks (24), the number of central nuclei in the gastrocnemius increased by 1.8-fold in $Acsl1^{M-/-}$ mice but did not change in littermate controls. These changes were not observed in $Acsl1^{M-/-}$ soleus, which had comparatively few central nuclei at rest or after exercise. Thus, the *Acsl1* deletion had a greater impact on glycolytic than oxidative fibers (Fig. 4, *D* and *F*). Immunohistochemical staining of the mitosis marker phosphohistone H3 supports the interpretation that the central nuclei were caused by regeneration (Fig. 4*G*), and compared with controls, the expression of the muscle regeneration markers *Myog* and *Myod*, respectively, in $Acsl1^{M-/-}$ muscle was 2.2- and 1.7-fold greater in white gastrocnemius, 61 and 28% lower in red gastrocnemius, and unchanged in soleus (Fig. 4*H*). These changes suggest that regeneration occurred almost exclusively in glycolytic skeletal muscle. Taken together, the results support the conclusion that ACSL1-directed FAO is required to maintain normal homeostasis in glycolytic muscle, particularly during exercise.

ACSL1 skeletal muscle deficiency induces apoptosis

Central nuclei occur when stem cells repair damaged muscle fibers (25). Muscle histology revealed no evidence of necrosis, and whereas *cleavage* of the apoptosis marker caspase-3 is generally accepted as a clear indication of apoptosis activation, increased expression of caspase-3 strongly correlates with the presence of apoptotic myonuclei in patients with Duchenne muscular dystrophy (26). Because caspase-3 protein is not observed in skeletal muscle from control mice, its appearance strongly suggested that $Acsl1^{M-/-}$ gastrocnemius cells were undergoing apoptosis (Fig. 5*A*) (27, 28). Although Western blotting analyses did not detect cleaved caspase-3 in gastrocnemius homogenates, positive cleaved caspase-3 was observed by immunohistochemical staining (Fig. 5*B*). In addition, the macrophage surface marker F4/80 was present in $Acsl1^{M-/-}$ gastrocnemius (Fig. 5*C*) in the absence of expression of the inflammatory markers, IL-1, IL-6, and tumor necrosis factor α (Fig. S4, *A* and *B*), consistent with the interpretation that macrophages were phagocytosing apoptotic myocytes.

Deletion of skeletal muscle Acsl1 induced mitochondrial biogenesis and oxidative fiber switching

In contrast to cardiac ACSL1, which prefers linoleate (18:2) as a substrate (17), skeletal muscle ACSL1 showed no distinct preference for linoleate, and the specific activity of acyl-CoA synthetase was least with oleate (18:1) (Fig. 6*A*). Similar to heart, ACS-specific activity and ACSL1 protein expression were enriched in mitochondrial membranes compared with homogenate (Fig. 6, *B* and *C*). Although additional fractionation studies showed some ACSL1 protein in ER, the presence of VDAC in the ER fraction indicated considerable mitochondrial contamination (data not shown). To assess the effect of ACSL1 loss on skeletal muscle mitochondria, we quantified the ratio of DNA copy number for NADH dehydrogenase 1 (*Nda1*) to the nuclear gene H19 (*H19*) (29). Compared with controls, mitochondrial content in $Acsl1^{M-/-}$ white gastrocnemius was 1.5-fold greater, but no difference was observed in red gastrocnemius or soleus (Fig. 6*D*). Similar to $Cpt1b^{M-/-}$ mice (21), the expression of mitochondrial FAO genes in gastrocnemius (Fig. 6*E*), but not soleus (Fig. 6*F*), increased ~2-fold, suggesting that the diminished FAO in $Acsl1^{M-/-}$ gastrocnemius promoted a compensatory increase in FAO capacity. Consistent with the increase in mitochondrial density, the inner mitochondrial enzyme, succinate dehydrogenase, was 1.5-fold greater in $Acsl1^{M-/-}$ gastrocnemius than in controls (Fig. 6*G*), indicating

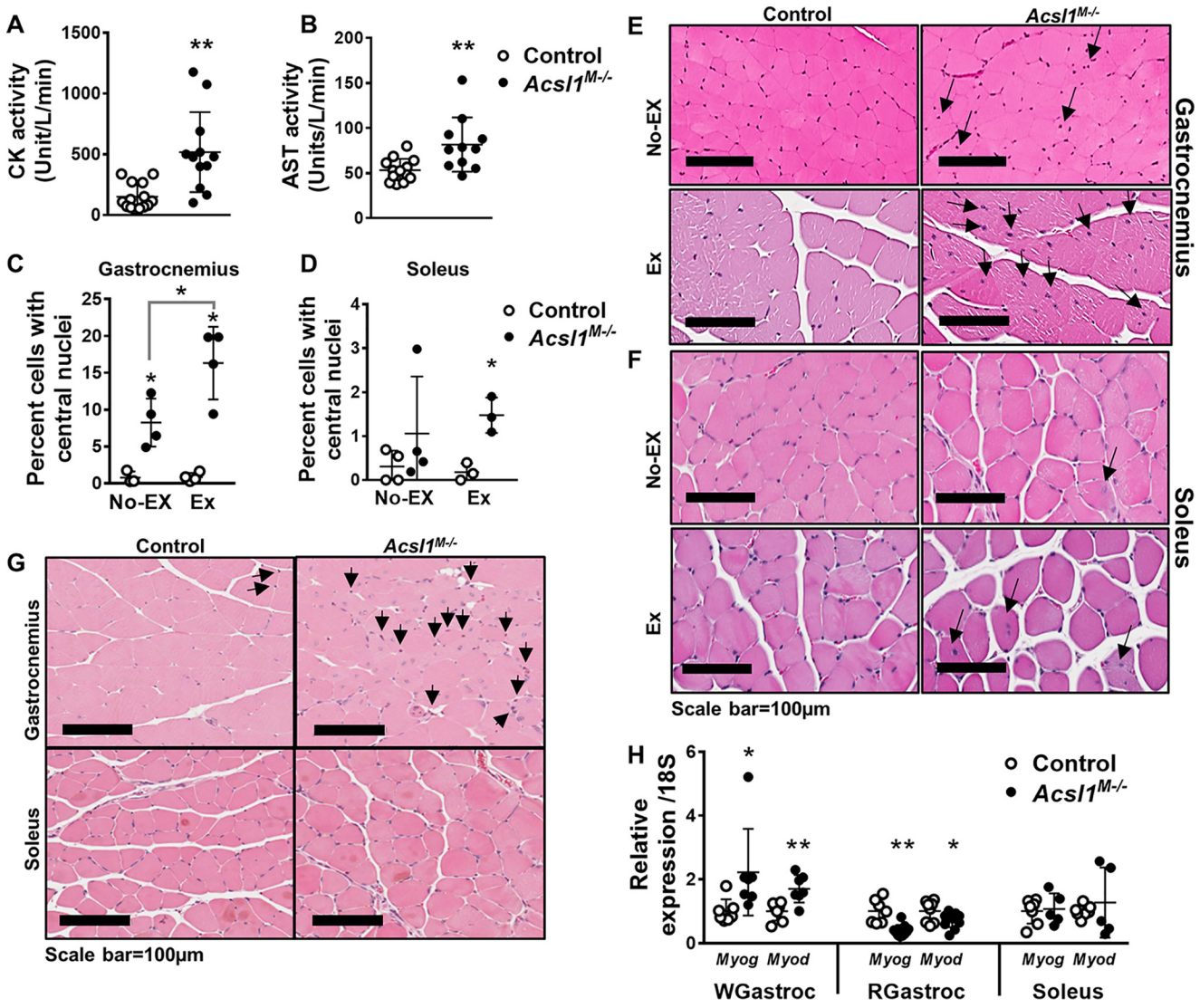

Figure 4. Myopathic features of *Acsl1*$^{M-/-}$ mice. Plasma creatine kinase (*CK*) (*A*) and aspartate transaminase (*AST*) (*B*) activities after food deprival for 4 h, $n = 11–14$ per genotype. *C* and *D*, approximately 2000 cells (total) from four randomly selected areas in two adjacent gastrocnemius sections and all cells from an entire soleus section were counted. Shown is the percentage of cells containing central nuclei in gastrocnemius and soleus from nonexercised (*No Ex*) and exercised (*Ex*) mice after 2 weeks of voluntary running, $n = 3–4$ per genotype. *E* and *F*, representative 100-μm images of hematoxylin and eosin–stained gastrocnemius and soleus. *Arrows*, central nuclei. *G*, tissue was fixed in 10% formalin. Representative 100-μm images of the immunostained mitosis marker, phosphohistone H3, in nonexercised gastrocnemius and soleus. *H*, mRNA expression of muscle regeneration markers *Myog* and *Myod* in white gastrocnemius (*WGastroc*), red gastrocnemius (*RGastroc*), and soleus. Data were normalized to 18S mRNA, $n = 5–7$ per genotype. Data are presented as means ± S.D. (*error bars*); **, $p < 0.01$; *, $p < 0.05$.

an increased percentage of oxidative fibers in *Acsl1*$^{M-/-}$ gastrocnemius (Fig. 6*H*) (30). Similarly, expression of the oxidative muscle marker *MhcI* (2) showed a 6.6-fold increase in *Acsl1*$^{M-/-}$ white gastrocnemius, but not in red gastrocnemius or soleus (Fig. 6*I*). Increases in mitochondria number and in oxidative muscle fibers are also seen with PGC1α activation (31). Compared with controls, *Ppargc1*α gene expression in ACSL1-deficient white gastrocnemius was slightly increased but did not reach significance, whereas *Ppargc1*α gene expression decreased in oxidative red gastrocnemius (Fig. 6*J*). The mRNA expression of PPARδ, which mediates the posttranscriptional increase of PGC-1α (32), did not increase in *Acsl1*$^{M-/-}$ mice, suggesting that it was not playing a major role in these changes (Fig. S4*D*). Taken together, these data suggest that loss of skeletal muscle ACSL1 promoted a compensatory increase in skeletal muscle mitochondrial biogenesis and FAO capacity that was more pronounced in glycolytic than oxidative skeletal muscle.

Deletion of skeletal muscle Acsl1 alters mitochondrial morphology but does not impair mitochondrial function

To determine whether loss of ACSL1 in skeletal muscle impaired mitochondrial function, as observed in ACSL1-deficient hearts (15), we measured the O_2 consumption rate (OCR) in isolated mitochondria by Seahorse analysis with pyruvate and malate (complex I substrates) or succinate and rotenone (complex II substrate plus complex I inhibitor). We detected no genotype-specific differences under either basal or ADP- or carbonyl cyanide-4-(trifluoromethoxy)-phenylhydrazone (FCCP)–stimulated states, indicating that despite a 90% reduction in FAO, mitochondria from *Acsl1*$^{M-/-}$ muscle functioned normally under resting conditions (Fig. 7, *A* and *B*). However, because *Acsl1*$^{M-/-}$ mice are

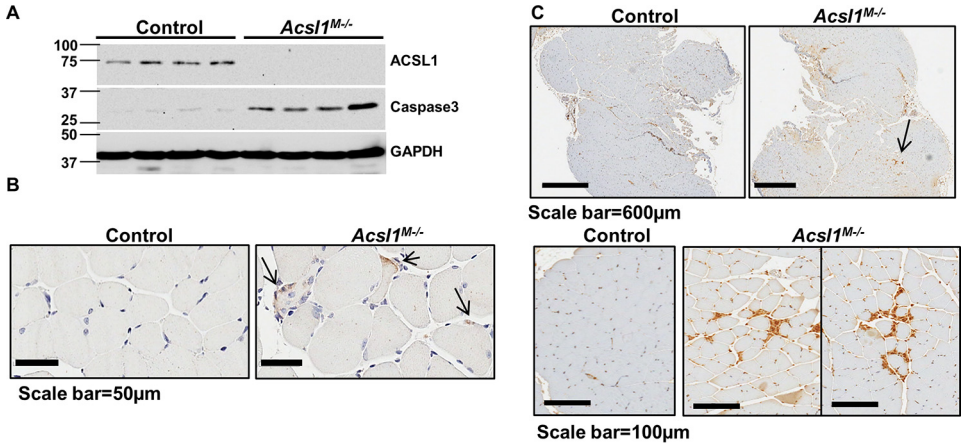

Figure 5. Deletion of *Acsl1* resulted in skeletal muscle cell apoptosis. *A*, mice were deprived of food for 4 h, muscles were excised, and muscle homogenates were subjected to Western blot analysis and immunoprobed with anti-caspase-3 and anti-GAPDH. *B*, gastrocnemius was fixed in 10% formalin and immunostained with anti-cleaved caspase-3. Shown are representative 50-μm images of immunostained cleaved caspase-3. *C*, representative images of gastrocnemius immunostained with anti-F4/80, a macrophage cell surface marker.

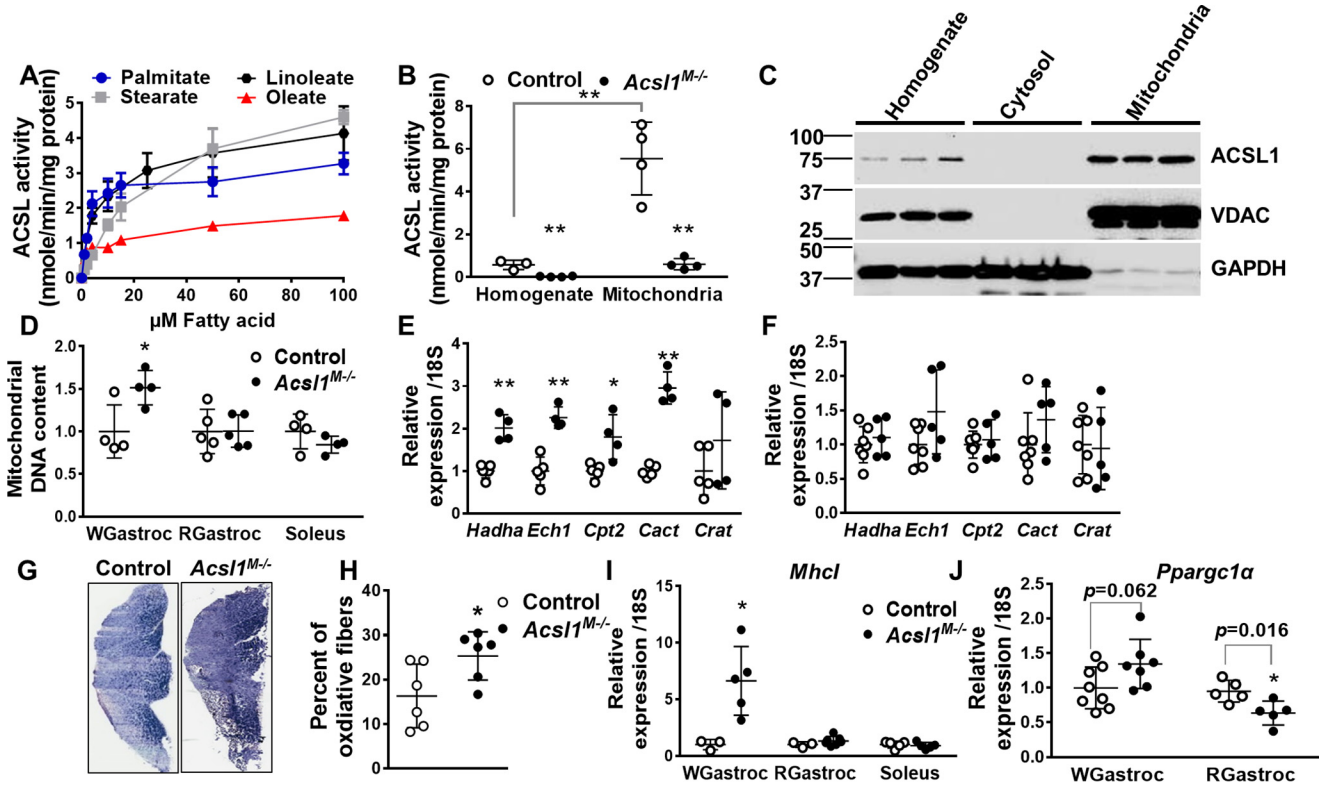

Figure 6. Deletion of *Acsl1* promoted compensatory mitochondrial biogenesis in glycolytic fibers. *A*, ACSL activity in total membrane fractions (10 μg of protein) measured with different concentrations of palmitate, stearate, linoleate, or oleate, $n = 3$ per genotype. *B*, ACSL activity in muscle homogenates and mitochondrial fractions measured with 50 μM palmitate, $n = 3$–4 per genotype. *C*, gastrocnemius total homogenate, cytosol, and mitochondria subjected to Western blotting and immunoprobed with anti-ACSL1, anti-VDAC, and anti-GAPDH. *D*, relative mitochondrial DNA content in white gastrocnemius (*WGastroc*), red gastrocnemius (*RGastroc*), and soleus. Data were normalized to genomic DNA H19, $n = 4$–5 per genotype. *E* and *F*, mRNA expression of fatty acid oxidation genes in gastrocnemius ($n = 4$–5 per genotype) (*E*) and soleus ($n = 5$–7 per genotype) (*F*). Data were normalized to 18S mRNA. *G*, representative images of succinate dehydrogenase staining in gastrocnemius. *H*, percentage of oxidative muscle fibers in gastrocnemius, $n = 6$ per genotype. *I*, mRNA expression of *Mhcl* in white gastrocnemius, red gastrocnemius, and soleus. Data were normalized to 18S mRNA, $n = 3$–7 per genotype. *J*, *Ppargc1* mRNA expression in white and red gastrocnemius. Data were normalized to 18S mRNA, $n = 5$–8 per genotype. Data are presented as means ± S.D. (*error bars*). **, $p < 0.01$; *, $p < 0.05$.

intolerant to endurance exercise (16) and had impaired voluntary running capacity and an exercise-induced increase in the percentage of central nuclei, we questioned whether exercise would affect mitochondrial function. After mice were allowed use voluntary running wheels for 1 week, the OCR in isolated mitochondria was similar between genotypes (Fig. 7, *C* and *D*), indicating normal mitochondrial function even after exercise.

Although the loss of skeletal muscle ACSL1 did not cause measurable mitochondrial dysfunction, the total mitochondria pellet size and the content of mitochondrial protein from ACSL1-deficient gastrocnemius was 13% lower (Fig. 7*E*), despite evidence for up-regulated mitochondrial biogenesis (Fig. 6, *D*–*J*). Because mitochondrial preparations tend to capture well-coupled and intact mitochondria and eliminate mito-

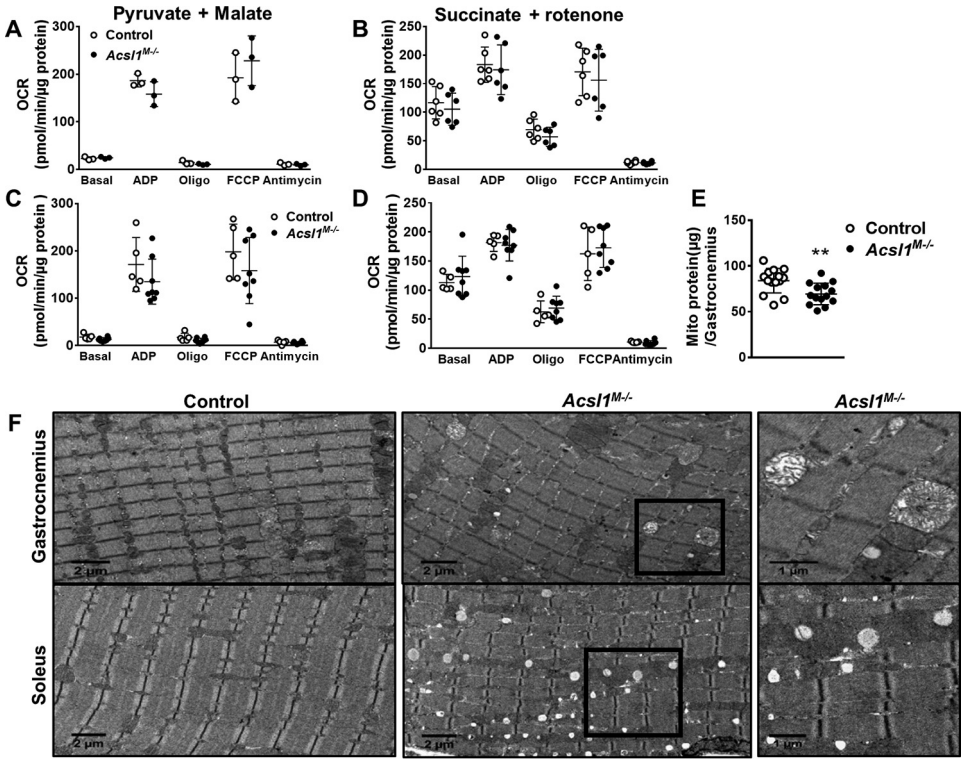

Figure 7. Deletion of *Acsl1* impaired mitochondrial morphology but not function. Mice were food-deprived for 3 h, and OCR was measured in isolated mitochondria from gastrocnemius with malate and pyruvate ($n = 3$ per genotype) (*A*) or succinate ($n = 6$ per genotype) (*B*) as substrates for either complex I or complex II. *C* and *D*, mice were allowed access to a voluntary running wheel for 1 week. Then mice were food-deprived for 3 h, and OCR was measured in isolated mitochondria with malate and pyruvate (*C*) or succinate (*D*), as substrates ($n = 5–8$ per genotype). *E*, mitochondrial protein content per gastrocnemius, $n = 14$ for each genotype. *F*, representative EM images from control and $Acsl1^{M-/-}$ gastrocnemius and soleus muscles. Data are presented as means ± S.D. (*error bars*). **, $p < 0.01$.

chondria that are flawed (33), we hypothesized that the mitochondria isolation protocol might have selectively excluded damaged mitochondria. Although the mitochondria isolated from control and $Acsl1^{M-/-}$ gastrocnemius showed equivalent membrane integrity as assessed by cytochrome *c* oxidase activity in the presence and absence of the detergent, *n*-dodecyl β-D-maltoside (data not shown), the 13% lower protein content (Fig. 7*E*) and reduced mitochondrial pellet size suggest that some damaged mitochondria had been eliminated. Although this limitation may have precluded full measurement of mitochondrial function, the small difference in protein recovery is unlikely to have markedly influenced functional measures.

Electron micrographs showed many swollen mitochondria with abnormal cristae in gastrocnemius from $Acsl1^{M-/-}$ mice (Fig. 7*F*), but swollen mitochondria were largely absent in $Acsl1^{M-/-}$ soleus. Whereas changes in mitochondria in soleus were not prominent, EM was consistent with the 2.5-fold higher TAG content (Fig. 2*A*) and excess lipid droplets observed with ORO staining (Fig. 1*E*). Thus, our data indicate that despite apparently normal OCR in isolated mitochondria, the lack of skeletal muscle ACSL1 resulted in disordered mitochondrial structure in glycolytic muscle.

Differences in phospholipid species from cardiac-specific and skeletal muscle–specific ACSL1-deficient mice

Changes in phospholipid composition may impair muscle function (34), and muscle cardiolipin content is particularly important for mitochondrial oxidative function (35). ACSL1 deficiency in heart markedly diminished the major cardiolipin (CL) species tetralinoleoyl-cardiolipin (17), but cardiolipin species in control and $Acsl1^{M-/-}$ gastrocnemius and soleus muscles were similar (Figs. S5 and S6). For other major phospholipids, the total content of each phospholipid was equivalent, but some differences were observed in selected acyl species. In both ACSL1-deficient gastrocnemius and soleus, the amounts of 34:1 phosphatidylcholine (PC) and 36:1 PC were greater, whereas 38:6 PC was lower. These changes in phospholipid species differed from those observed in ACSL1-deficient hearts, indicating that the effects of ACSL1 deficiency on PC species are tissue/organ-specific. Phospholipid species also differed between the gastrocnemius and soleus muscles themselves. Interestingly, however, deficiency of ACSL1 resulted in similar changes in phosphatidylinositol species in heart and soleus; both organs showed increases in 36:3 and 38:5 and a 50% lower content of 38:4, the major PI species (specifically identified as 18:0, 20:4 in heart) (17).

Skeletal muscle ACSL1 deficiency causes increased protein turnover in glycolytic but not oxidative muscle fibers

Because the loss of ACSL1 reduced palmitate oxidation by 90% in gastrocnemius while having no apparent effect on glucose uptake or use, we hypothesized that $Acsl1^{M-/-}$ skeletal muscle must rely on energy either produced from elevated peroxisomal FAO or derived from the catabolism of muscle protein. In contrast to $Cpt1^{M-/-}$ mice (21), however, the expression of mRNAs related to peroxisomal FAO was similar in

gastrocnemius from *Acsl1*$^{M-/-}$ and control mice (Fig. S4*C*), and long-chain FAO was less than 10% of controls. These features suggested that peroxisomal FAO had not increased in ACSL1-deficient muscle. Thus, muscle must use amino acids as fuel to accommodate its energy demand. Protein turnover rates are accelerated in several myopathies. In Mdx mice, a model of Duchenne muscular dystrophy, for example, gastrocnemius protein turnover is greater than in controls (36, 37), and protein turnover rates are greater in severely affected patients with limb girdle muscular dystrophy (38). The muscle-specific deletion of *Acsl1* did not result in an increased size of gastrocnemius relative to body weight or an increase in myocyte cross-sectional area (Fig. S7, *A* and *C*). Thus, neither hypertrophy nor atrophy was present in gastrocnemius, although the much smaller soleus muscle increased both weight and myocyte size (Fig. S7, *B* and *D*). Protein turnover rate is determined by the rates of protein synthesis and protein degradation. To assess the rate of protein synthesis in *Acsl1*$^{M-/-}$ skeletal muscle, we performed a SUnSET assay in which puromycin, an aminoacyl-tRNA analog, is incorporated into newly synthesized protein, thereby both blocking protein elongation and serving as an indicator of new protein synthesis via immunodetection of puromycin-labeled peptides (39). In nonexercised mice, the rates of new protein synthesis in *Acsl1*$^{M-/-}$ and control gastrocnemius and soleus were similar (Fig. S8, *A* and *B*). Because the rate of protein synthesis increases after both resistance and endurance training (40–42), we exercised mice on a treadmill for 45 min at 12 m/min (~500 meters), a period of exercise that does not cause early exhaustion in *Acsl1*$^{M-/-}$ mice from hypoglycemia (plasma glucose 128 and 134 mg/dl in *Acsl1*$^{M-/-}$ and controls, respectively; $n = 3$ per genotype) (16). Immediately afterward, we injected puromycin intraperitoneally (IP) to examine the rate of new protein synthesis (Fig. 8, *A* and *B*). The amount of puromycin incorporated was 2.1-fold greater in *Acsl1*$^{M-/-}$ glycolytic white gastrocnemius than in controls, but no difference was observed in red gastrocnemius or soleus, indicating that, similar to the presence of central nuclei and the expression of *Myog* and *Myod*, the change was more pronounced in glycolytic muscle fibers. At this time point, a 2.5-fold increase in pS6 kinase phosphorylation exclusively in white gastrocnemius indicated the presence of activated mTORC1 (Fig. 8, *C* and *D*) in glycolytic muscle, consistent with the increased rate of protein synthesis. Increased p62 in white gastrocnemius indicated a concomitant block in autophagy (Fig. 8, *E* and *F*). Although ubiquitinated proteins did not differ between the two genotypes 30 min after exercise (Fig. S9), it is possible that measurement at a different time point might confirm increased proteolysis; alternatively, a ubiquitin-independent proteolytic pathway may be active. Supporting this interpretation are previously reported data showing decreases in most muscle amino acids after *Acsl1*$^{M-/-}$ mice are exercised, as well as increased gastrocnemius content of acyl-carnitine metabolites of branched-chain amino acid degradation (16).

Discussion

ACSL1-activated fatty acids are specifically directed toward mitochondrial β-oxidation in highly oxidative tissues, including skeletal muscle (16, 43). Lack of ACSL1 in skeletal muscle reduces endurance exercise capacity and impairs metabolic homeostasis (16). What is less evident is the extent of the impairment and the mechanism that damages muscle when FAO is insufficient for energy production. Compared with controls, mice lacking ACSL1 in skeletal muscle had impaired physical performance, together with muscle damage, apoptosis, and induced regeneration. These findings, as well as increased mitochondrial biogenesis, likely resulted from a continued reduction of muscle protein and were more evident in glycolytic than oxidative muscle.

In the heart, fatty acids are the primary fuel, and lack of myocardial ACSL1 activates the mTORC1 pathway, resulting in cardiac hypertrophy and a block in mitophagy (15). FAO is also the primary energy source in skeletal muscle, both at rest and during sustained exercise. In contrast to *Acsl1*-deficient hearts, however, *Acsl1*$^{M-/-}$ gastrocnemius weight did not increase, indicating a lack of hypertrophy despite mTORC1 activation. Thus, the absence of ACSL1, despite an equivalent reduction in FAO, results in different outcomes in heart and skeletal muscle. These different responses to defective FAO were likely due to compensatory differences in fuel use in the two tissues. In ACSL1-deficient heart, uptake of the glucose analog 2-[1-^{14}C]deoxyglucose increases 8-fold and glucose 6-phosphate content increases 3-fold, indicating a marked reliance on glucose in the absence of FAO (15, 44). In contrast, glucose uptake did not increase in skeletal muscle from shivering *Acsl1*$^{M-/-}$ mice. In fact, when excess glucose was provided during a hyperinsulinemic-hyperglycemic clamp, *Acsl1*$^{M-/-}$ skeletal muscle took up less glucose than controls, and less glucose was required to maintain the plasma glucose concentration at 225 mg/dl, suggesting that *Acsl1*$^{M-/-}$ mice are mildly insulin-resistant. This interpretation seems to conflict with our previous finding that, compared with controls, insulin stimulation results in enhanced Akt phosphorylation in *Acsl1*$^{M-/-}$ gastrocnemius. The discrepancy suggests that Akt activation was insufficient to increase glucose uptake. A similar finding was reported in patients with a myopathy imposed by critical illness (45). In that study, GLUT4 was ineffectively translocated to the muscle sarcolemma membrane despite Akt activation. Taken together, our data indicate that in *Acsl1*$^{M-/-}$ mice, the reduction in mitochondrial FAO did not result in enhanced skeletal muscle glucose disposal despite enhanced Akt phosphorylation.

Because long-chain acyl-CoAs must be converted to acylcarnitines before they can be oxidized, the absence of muscle CPT1b blocks FAO and initiates an adaptive response that includes mitochondrial biogenesis, compensatory peroxisomal FAO, increased carbohydrate use, and enhanced amino acid catabolism (21). During both exercise and fasting, normal skeletal muscle oxidizes fatty acids and releases amino acids that are used for hepatic gluconeogenesis, thereby allowing the maintenance of normal blood glucose levels (46). Although the role of ACSL1 in providing activated long-chain acyl-CoAs for FAO would appear to be similar to that of CPT1, compensatory fuel use differs markedly. *Acsl1*$^{M-/-}$ mice rapidly deplete muscle glycogen stores, but muscle use of exogenous glucose does not increase (16). Thus, because the hypoglycemia that develops in *Acsl1*$^{M-/-}$ mice after an overnight fast or endurance exercise is

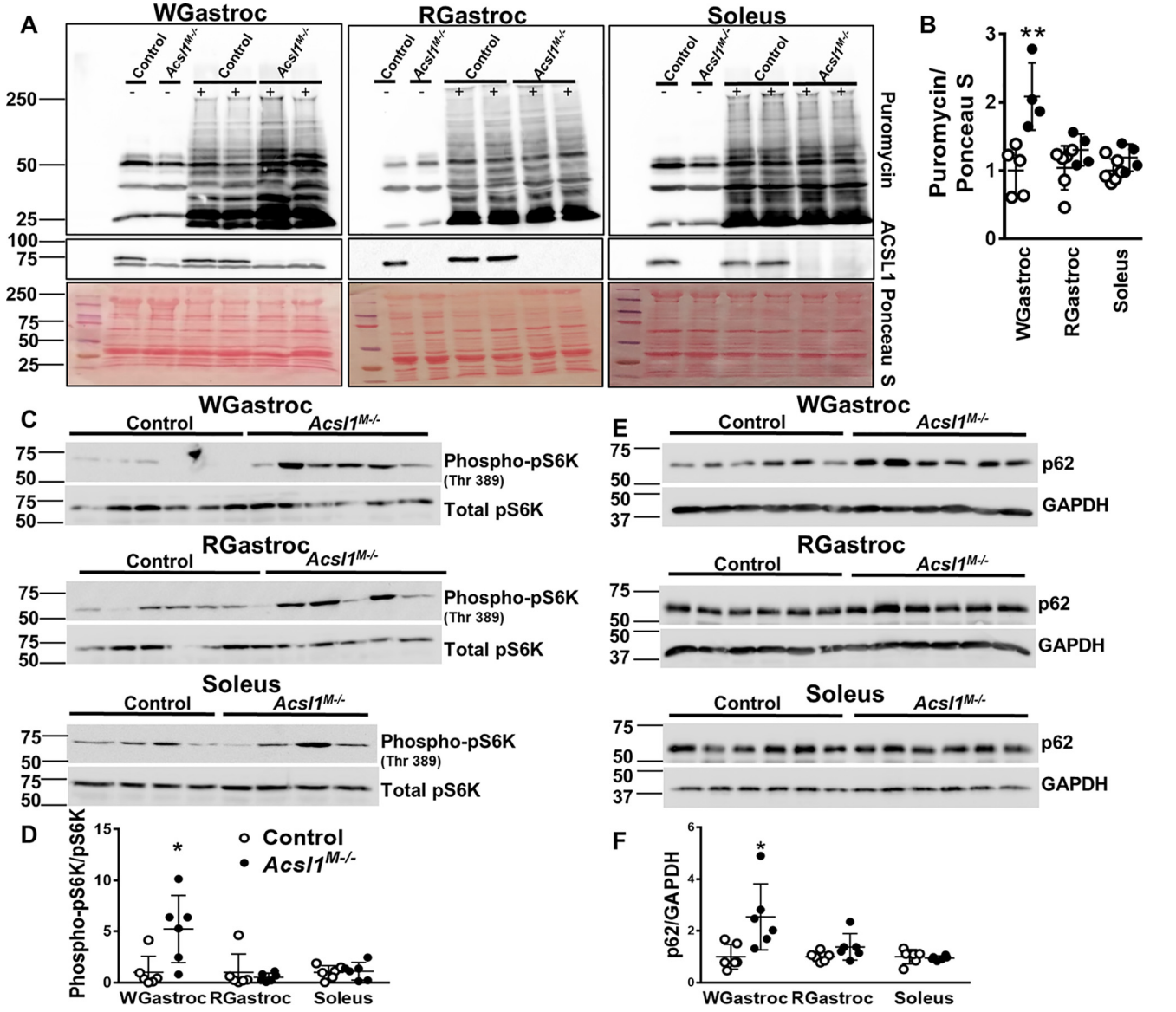

Figure 8. Deletion of *Acsl1* increased protein synthesis in glycolytic muscle after endurance exercise. Mice were exercised on a treadmill for 45 min, and sterilized puromycin solution in water (0.04 μmol/g) was injected IP immediately afterward. White gastrocnemius (*WGastroc*), red gastrocnemius (*RGastroc*), and soleus were collected 30 min later and homogenized. Homogenates were then probed with anti-puromycin and anti-ACSL1 antibodies. ImageJ software was used to quantify relative pixel density of the bands. *A*, representative Western blots of anti-puromycin and anti-ACSL1 (−, no puromycin injection; +, puromycin injection), and membranes were stained with Ponceau S. *B*, quantitation of puromycin incorporation normalized to Ponceau S, $n = 4–5$ per genotype. *C*, Western blots of anti-phospho-pS6K and anti-total pS6K in white gastrocnemius and red gastrocnemius. Representative Western blotting of anti-phospho-pS6K and anti-total pS6K in soleus. *D*, quantitation of pS6K phosphorylation, $n = 6$ per genotype. *E*, Western blots of anti-p62 and anti-GAPDH in white gastrocnemius, red gastrocnemius, and soleus. *F*, quantitation of p62 was normalized to GAPDH, $n = 6$ per genotype. Data are presented as means ± S.D. (*error bars*). *, $p < 0.05$; **, $p < 0.01$.

not due to increased skeletal muscle glucose uptake, we inferred that it must result from reduced hepatic glucose production resulting from insufficient availability of gluconeogenic amino acids (16). Supporting this interpretation are our previous findings that, compared with controls, fasted *Acsl1*$^{M-/-}$ mice produce more glucose from glycerol, indicating a greater capacity for hepatic gluconeogenesis, and the observed lower content of free amino acids in ACSL1-deficient muscle (16).

With an inability to use either fatty acids or glucose effectively for energy, *Acsl1*$^{M-/-}$ muscle must therefore depend on increased protein degradation to release amino acids for oxidation. Exercise activates muscle glycogenolysis, the tricarboxylic acid cycle, and amino acid uptake, and in both humans and rats after mild resistance exercise (40) or after endurance exercise such as running or cycling (41, 42), the rate of muscle protein synthesis increases. When we exercised mice on a treadmill, the rate of protein synthesis increased 2-fold in *Acsl1*$^{M-/-}$ glycolytic muscle, an effect that was not observed in oxidative muscles. Together with our previous finding that ACSL1-deficient muscle had a 30% reduction of total free amino acids after endurance training (16), this finding suggests why the release of amino acids is inadequate for hepatic gluconeogenesis.

Skeletal muscle can oxidize only six amino acids, the branched-chain amino acids (BCAAs) leucine, isoleucine, and valine, plus glutamate, aspartate, and asparagine (47). BCAAs account for 14–18% of total amino acids and 35% of essential

amino acids in skeletal muscle where BCAAs are primarily oxidized (48, 49). The continued drain on muscle protein, especially of BCAAs, is likely to be responsible for the myopathy observed in $Acsl1^{M-/-}$ mice. Branched-chain α-keto acid dehydrogenase complex (BCKDH) regulates the rate-limiting step of BCAA degradation (47). In both human and rodent skeletal muscle, exercise activates BCKDH and depletes glycogen (47, 50). In glycogen-depleted muscle, enhanced leucine oxidation results in a net carbon drain on the tricarboxylic acid cycle, eventually leading to muscle fatigue (47). We speculate that lack of ACSL1 increased the metabolism of muscle BCAAs and explains the muscle pathology. Given that BCAA supplementation increases both muscle and arterial BCAA concentrations and prevents muscle protein degradation during exercise (48, 50), studying the effect of BCAA supplementation may be warranted to determine whether the $Acsl1^{M-/-}$ myopathy might improve. BCAAs are ketogenic. Despite the fact that exercise increases BCAA oxidation, we found that plasma β-hydroxybutyrate in $Acsl1^{M-/-}$ mice and controls is similar (16), suggesting that ketones might also be used as a muscle energy source. Full-length caspase-3 was expressed only in $Acsl1^{M-/-}$ skeletal muscle, and cleaved caspase-3, which plays a major role in inducing both the intrinsic and extrinsic apoptosis pathways (27), was present only in $Acsl1^{M-/-}$ skeletal muscle. After apoptotic cell death, inflammatory cells migrate to the injured locus and remove debris to allow the normally quiescent satellite cells to proliferate and differentiate into mature myoblasts, which then fuse with each other and with surviving fibers to repair myocytes (51, 52). Positive immunostaining of cleaved caspase-3, as well as evidence of macrophage infiltration, supports the interpretation that apoptosis underlies muscle cell death in $Acsl1^{M-/-}$ gastrocnemius. The marked increase in the number of central nuclei in $Acsl1^{M-/-}$ gastrocnemius after exercise together with increased mRNA expression of the regeneration markers *Myod* and *Myog* and positive staining of the mitosis marker phosphohistone H3 is indicative of robust muscle regeneration.

Although ACSL1 deficiency resulted in a 90% reduction in FAO in red gastrocnemius and a 77% reduction in white gastrocnemius, the major molecular and histological changes occurred in the more glycolytic white gastrocnemius. Thus, white gastrocnemius had more damaged fibers and up-regulated expression of oxidative genes, suggesting an attempt to increase oxidative capacity. The mRNA expression of *MhcI*, a marker of oxidative muscle fibers, increased 6-fold in white gastrocnemius. White gastrocnemius also showed up-regulation of genes related to mitochondrial FAO, increased mitochondrial copy number, and a greater amount of oxidative muscle fibers, as evidenced by SDH staining. These changes suggest that $Acsl1^{M-/-}$ muscle responded to reduced FAO by increasing mitochondrial biogenesis and switching fiber type from glycolytic to oxidative. Similar changes have also been observed in mice lacking very-long-chain acyl-CoA dehydrogenase ($VLCAD^{-/-}$), which catalyzes the first of four sequential reactions in the mitochondrial oxidation of long-chain fatty acids (53). Like $Acsl1^{M-/-}$ muscle, $VLCAD^{-/-}$ muscle increases mRNA expression of the oxidative muscle marker troponin I (54). Despite the increase in $Acsl1^{M-/-}$ mitochondrial content, however, mitochondrial OCR was similar in both genotypes, with the caveat that the mitochondria isolation procedure may have selectively excluded damaged mitochondria present in $Acsl1^{M-/-}$ muscle.

The oxidative soleus muscle was protected from the defects observed in glycolytic white gastrocnemius. Compared with controls, the ratio of $Acsl1^{M-/-}$ soleus weight to total body weight was significantly greater, and cell size was larger, in part because of an accumulation of TAG. Compared with gastrocnemius, fewer $Acsl1^{M-/-}$ soleus myocytes contained central nuclei and, unlike gastrocnemius, the number of central nuclei increased only minimally after exercise. In addition, no changes were observed in expression of muscle regeneration markers or markers for enhanced mitochondrial biogenesis. Why soleus was protected remains unclear.

Muscle type–specific differences are present in several muscle disorders. For example, in a mouse model of spinal bulbar muscular atrophy deficiency, in patients with Duchenne muscular dystrophy, and in Mdx mice, glycolytic muscles are most severely affected, and metabolic changes are characterized by a switch in fiber type from glycolytic to oxidative (55–57). Gastrocnemius consists of a mix of oxidative and glycolytic fibers, whereas soleus is composed primarily of oxidative fibers. The mRNA expression of genes linked to fatty acid transport and TAG synthesis is greater in soleus than in the extensor digitorum longus, a predominantly glycolytic muscle, suggesting that soleus has a greater capacity for lipid accumulation (58). Despite a 72% decrease in total ACS activity compared with controls, ACSL1-deficient soleus contained 2.5 times more TAG. The accumulation of excess fatty acids in the TAG pool is believed to sequester lipid molecules and divert them from potentially lipotoxic pathways; thus, the presence of lipid droplets may explain why less damage was observed in $Acsl1^{-/-}$ soleus (59). In addition, metabolically active intramyocellular lipid droplets are frequently observed adjacent to mitochondria. These lipid droplets serve as metabolic fuel during exercise or fasting (58, 60). Compared with red or white gastrocnemius, total ACS activity in soleus was 2- and 4-fold higher, respectively. In $Acsl1^{-/-}$ muscles, ACS activity decreased by more than 90%, although residual activity remained highest in soleus, and palmitate oxidation was only 72% lower than in controls. Our observation that ACSL3 mRNA expression was 3.4-fold higher in $Acsl1^{M-/-}$ compared with controls suggests that ACSL3 may be compensating for the deficiency in ACLS1. *Acsl3* mRNA also increased in hearts lacking ACSL1 (18). The specific function of ACSL3 has not been determined, but it has been implicated in the synthesis of PC (61) and in the KRAS-mediated production of acyl-CoAs that are directed toward β-oxidation in lung cancer cells (62). Together, these data suggest that lack of ACSL1-dependent fatty acid metabolism is more problematic in glycolytic than oxidative muscle.

Compared with controls, the rate of protein synthesis was 2.1-fold greater after exercise in $Acsl1^{M-/-}$ glycolytic muscle, consistent with the need to resynthesize protein that had been degraded to supply amino acids for fuel. The drain of muscle amino acids for potential local utilization as fuel and protein resynthesis reduced the pool of muscle free amino acids, diminishing their release as substrates for hepatic gluconeogenesis.

Taken as a whole, our data suggest that FAO is critical for normal skeletal muscle homeostasis during both rest and activity; the resulting overall deficit in muscle fuel availability causes a myopathy manifested by exercise intolerance, muscle weakness, and myocyte apoptosis.

Experimental procedures

Animal studies

Studies were performed with approval of and in accordance with the guidelines of the Institutional Animal Care and Use Committee at the University of North Carolina at Chapel Hill. Mice were housed in a climate-controlled animal facility with *ad libitum* access to food (Prolab RMH 3000 SP76 chow) and water. Littermate $Acsl1^{flox/flox}$ (63) mice served as controls. $Acsl1^{M-/-}$ mice were generated by crossing $Acsl1^{flox/flox}$ mice with mice expressing muscle-specific human skeletal actin promoter (Jackson Laboratory, catalog no. 006149)-driven Cre recombinase (16). Mice were backcrossed six times onto the C57BL6/J background. 3–4-Month old mice were studied. We previously reported that measurements were qualitatively similar between male and female $Acsl1^{M-/-}$ mice (16), so we have reported the majority of the measurements from only one sex. Red gastrocnemius samples included plantaris. Voluntary exercise was measured as described previously (64). Briefly, mice were housed in single cages with accessible individual running wheels for 14 consecutive days. Wheel-running activity was monitored and recorded at 1-min intervals. Running distance, average speed, maximal speed, and percent of time spent running were calculated. Activity during the light and dark cycles (720 min) was analyzed separately. Mice were stressed with treadmill exercise before measuring the rate of protein synthesis. Before exercise, mice were acclimated on a speed-controlled treadmill for 3 consecutive days as described (16). On the day of the experiment, mice were fasted for 2 h and placed on the treadmill. The treadmill protocol was programmed for a total of 45 min: 0–3 m/min for 30 s, 3–6 m/min for 90 s, 6–10 m/min for 90 s, 10 m/min for 900 s, 10–12 m/min for 60 s, and 12 m/min for 1500 s. For the final minute of the protocol, the speed was gradually reduced from 12 to 0 m/min (16). Immediately after exercise, a surface sensing of translation (SUnSET) assay was performed to assess the rate of global protein synthesis (39). For this study, sterilized puromycin (Sigma, 8833) in water (4 mg/ml) was injected IP. The body weight of the mouse was measured before the treadmill exercise, and the volume of puromycin was calculated as (body weight $\times$ 0.04 $\times$ 1000)/7.36 for a final concentration of 0.04 μmol/g. 30 min later, mice were anesthetized, and skeletal muscle was collected for Western blot analysis. For the wire hang grip test to assess muscle strength, individual mice were placed at the center of a large metal rat cage lid. Once the mouse had gripped the metal grid, the cage lid was inverted over a large foam pad and suspended 30 cm above the pad. The latency for the mouse to fall from the lid was recorded in seconds. Hanging was scored as follows: -4, falling from the lid within 30 s; -2, falling within 60 s or poor gripping, using the limbs or using two paws instead of four paws; 0, well-coordinated gripping with good turning ability; $+2$, superior coordination with smooth turning (65). A hyperinsulinemic-hyperglycemic clamp study was conducted by the Mouse Metabolic Phenotyping Center at Yale as described previously (66).

Metabolites

After 4 h of food deprivation, blood was collected by retro-orbital bleeding to measure plasma creatine kinase activity (CK Liqui-UV® test kit; Stanbio, catalog no. 2910) and aspartate aminotransferase activity (Liquid AST Reagent Set; Thermo Fisher Scientific, catalog no. 23-666-120). To measure glycogen, muscle was weighed and immediately snap-frozen in liquid nitrogen. Glycogen was measured by the acid hydrolysis method (16). Glucose was measured by Autokit Glucose (Wako Diagnostics, catalog no. 997-03001). Muscle lipid was extracted by the Folch method (67), and TAG content was measured colorimetrically (Sigma, catalog no. T2449).

Biochemical measurements

FAO was measured as described (15). Briefly, muscle was minced and homogenized in ice-cold buffer (100 mM KCl, 40 mM Tris-HCl, 10 mM Tris base, 5 mM $MgCl_2$, $6H_2O$, 1 mM EDTA, and 1 mM ATP (pH 7.4)) at a 10-fold dilution (w/v). Oxidation was measured for 30 min in a 200-μl reaction mixture containing 100 mM sucrose, 10 mM Tris-HCl, 10 mM KPO_4, 100 mM KCl, 1 mM $MgCl_2$, 1 mM L-carnitine, 0.1 mM malate, 2 mM ATP, 0.05 mM CoA, and 1 mM DTT (pH 7.4) with palmitate or pyruvate as substrate. Either the production of ^{14}C-labeled CO_2 plus acid-soluble metabolites or only the production of ^{14}C-labeled CO_2 was measured. To measure glucose uptake, mice were placed at 4 °C for 2 h and then injected IP with 10 μCi of 2-[1-^{14}C]deoxyglucose in saline. Skeletal muscles were harvested and snap-frozen in liquid N_2. Radioactivity was measured in tissue homogenates, and the result was normalized to the radioactivity in 10 μl of serum collected 5 min after injection (15).

ACS activity

Muscle ACS activity (initial rates) was measured as described (18). Briefly, tissue homogenates were centrifuged at 100,000 $\times$ *g* for 1 h at 4 °C to isolate total membrane fractions. Protein (2–15 μg) was incubated with 50 mM [1-^{14}C]palmitate, 175 mM Tris-HCl, pH 7.4, 10 mM ATP, 250 mM CoA, 5 mM DTT, and 8 mM $MgCl_2$ at room temperature for 10 min. The enzyme reaction was stopped with 1 ml of Dole's solution (heptane, isopropyl alcohol, 1 M H_2SO_4; 80:20:1, v/v/v). 2 ml heptane and 0.5 ml water were added to separate the phases. Radioactivity of the [1-^{14}C]palmitoyl-CoA in the aqueous phase was measured.

Immunoblots

Muscles were homogenized in lysis buffer (20 mM Tris, 1% Triton X-100, 50 mM NaCl, 250 mM sucrose, 50 mM NaF, 5 mM $Na_4P_2O_7$, and protease and phosphatase inhibitor mixture (Thermo Fisher Scientific, catalog no. 78422) with a motor-driven Teflon-glass homogenizer (Potter-Elvehjem, Pro Scientific Inc.). Total protein lysate was collected by centrifuging the homogenate at 700 $\times$ *g* for 5 min. Protein concentrations were measured by the BCA protein assay (Thermo Fisher Scientific, catalog no. 23225) and loaded on a 12% SDS gel. Primary anti-

bodies were used for caspase-3 (1:1000) (Cell Signaling Technology, catalog no. 9662), ACSL1 (1:1000) (Cell Signaling Technology, catalog no. 4047), GAPDH (1:20,000) (Abcam, ab8245), puromycin (1:1000) (Millipore Sigma, MABE343), VDAC (1:4000) (Abcam, 15859), ubiquitin (1:1000) (Cell Signaling Technology, catalog no. 3933S), phospho-p70 S6 kinase (1:1000) (Cell Signaling Technology, catalog no. 9234L), p70 S6 (1:1000) (Cell signaling Technology, catalog no. 2708S), and P62 (1:5000) (Abnova, H00008878-M01). Goat anti-mouse IgG (H+L) secondary antibody, horseradish peroxidase (Thermo Fisher Scientific, 31430), and goat anti-rabbit IgG (H+L) secondary antibody, horseradish peroxidase (Thermo Fisher Scientific, 31460) were used.

Histology

Muscles were either snap-frozen in liquid nitrogen–cooled isopentane or fixed in 10% neutral buffered formalin for paraffin embedding. Muscle tissues were sectioned by the UNC Histology Research Core Facility. For succinate dehydrogenase (SDH) staining, frozen sections were incubated with 0.0065% KCN, 0.185% EDTA, 0.1% nitro blue tetrazolium, and 50 mM sodium succinate for 3 min in a 37 °C incubator. Tissue sections were then washed with distilled H_2O and acetone and mounted (Shandon™ Immu-Mount™; Thermo Fisher Scientific, catalog no. 9990402). For Oil Red O (ORO) staining, frozen sections were incubated with freshly prepared ORO working solution (0.5% ORO in isopropyl alcohol diluted in water at a 3:2 ratio) for 15 min at room temperature. Tissue sections were rinsed with 60% isopropyl alcohol and water and counterstained with hematoxylin and then mounted with Shandon™ Immu-Mount™. Formalin-fixed paraffin-embedded sections were stained with anti-cleaved caspase-3 (1:1000 dilution) (Cell Signaling, 9661S) for apoptosis, anti-phosphohistone H3 (Ser-10) (1:400 dilution) (Cell Signaling, 9701S) for mitosis, or anti-F4/80 (1:200 dilution) (AbD Serotec/Bio-Rad, MCA497) for macrophage infiltration. The UNC Histology Research Core Facility performed immunohistochemistry and hematoxylin and eosin staining. All slides were scanned with an Aperio digital scanner. ImageJ software was used to set the threshold to quantify the percentage of oxidative fibers. Oxidative fibers were defined by the medium-to-dark blue colors (30). To determine the percentage of cells containing central nuclei, four different areas from the gastrocnemius (~2000 muscle fibers in total) and an entire soleus section were selected randomly and examined.

EM

EM was performed by the UNC Microscopy Service Laboratory (18). Mice were food-deprived for 4 h, and gastrocnemius and soleus were perfused and fixed with fresh 2.5% glutaraldehyde, 2% paraformaldehyde in 0.15 M sodium phosphate buffer, pH 7.4.

Analysis of gene expression and mitochondria copy number

Skeletal muscle total RNA was extracted (RNeasy Plus Mini Kit; Qiagen, catalog no. 74134) and reverse transcribed with the iScript cDNA synthesis kit (Bio-Rad, 1708890). DNA was isolated with the DNase Blood & Tissue Kit (catalog no. 69504). cDNA and DNA were amplified with iTaq™ Universal SYBR® Green Supermix (Bio-Rad, 1725121). Sequences of primers used in this study are listed (Table S1). The mitochondrial DNA gene NADH dehydrogenase 1 was normalized to nuclear DNA gene H19, and the ratio of mitochondria DNA copy number/nuclear DNA copy number was quantified as described (29).

Mitochondria studies

To isolate mitochondria, gastrocnemius was minced 200 times in ice-cold isolation buffer (70 mM sucrose, 210 mM mannitol, 5 mM HEPES, 1 mM EGTA, and 0.5% (w/v) fatty acid free BSA) immediately after dissection. Minced muscle was homogenized in a motor-driven Teflon-glass homogenizing vessel with 10 up-and-down strokes. The homogenate was centrifuged at 700 × *g* for 5 min at 4 °C to remove unbroken cells and nuclei. The supernatant was centrifuged at 8000 × *g* for 10 min at 4 °C to pellet mitochondria. To measure mitochondrial protein concentration and total mitochondrial protein amount per gastrocnemius, mitochondria were suspended in 100 μl of isolation buffer without BSA to avoid interference with the protein assay, and 10 μl of mitochondrial suspension was used to measure protein concentration by the Bradford method. The remaining 90 μl of the mitochondrial suspension was centrifuged for a second time at 8000 × *g* for 10 min at 4 °C. The mitochondrial pellet was resuspended in assay buffer containing 70 mM sucrose, 220 mM mannitol, 10 mM KH_2PO_4, 5 mM $MgCl_2$, 2 mM HEPES, 1 mM EGTA, and 0.2 (w/v) fatty acid-free BSA. The amount of total mitochondrial protein per gastrocnemius was calculated by multiplying the volume (90 μl) by the mitochondrial protein concentration (μg/μl). Mitochondrial OCR was measured with a Seahorse XF96 Analyzer with 5 mM pyruvate and 5 mM malate as complex I substrates, and 10 mM succinate plus 2 μM rotenone as complex II substrate and complex I inhibitor. Mitochondria (4 μg of protein) were stimulated in succession with 100 mM ADP, 1 mg/ml oligomycin, 4 mM FCCP, and 4 mm antimycin A, all of which were dissolved in assay buffer without BSA to avoid port injection failure (18). Mitochondrial outer membrane integrity was assessed by a cytochrome *c* oxidase assay kit according to the protocol (MilliporeSigma, CYTOCOX1).

Phospholipid analysis

Samples of soleus and gastrocnemius were prepared (18) with modifications. Tissues were homogenized with an Omni Bead Ruptor Elite in ice-cold PBS and protease inhibitors (Roche Applied Science). Protein was determined by the bicinchoninic acid method (Pierce). Homogenates (500 μg of protein) were diluted with PBS to a total volume of 200 μl. An internal standard mixture from Avanti Polar Lipids was resuspended and mixed in 100% methanol (50 ng of each phospholipid class, 100 ng of CL). This mixture contained 1,2-didodecanoyl-*sn*-glycero-3-phosphate (PA-12:0/12:0), 1,2-didodecanoyl-*sn*-glycero-3-phosphocholine (PC-12:0/12:0), 1,2-didodecanoyl-*sn*-glycero-3- phosphoethanolamine (PE-12:0/12:0), 1,2-didodecanoyl-*sn*-glycero-3-phosphoglycerol (PG-12:0/12:0), 1,2-dioctanoyl-*sn*-glycero-3-phosphoinositol (PI-8:0/8:0), 1,2-didodecanoyl-*sn*-glycero-3-phosphoserine (PS-12:0/12:0), and 1′-(1,2-di-(9*Z*-tetradecenoyl)-

sn-glycero-3-phospho), 3′-(1-(9*Z*-tetradecenoyl), 2-(10*Z*-pentadecenoyl)-*sn*-glycero-3-phospho)-*sn*-glycero (CL-(14:1) x3/15:1). Then 750 μl of methanol/chloroform (2:1; v/v) plus an internal standard mixture of 50 ng for each phospholipid class and 100 ng of CL was added, and products were extracted (68). Samples were dried under N_2 and then resuspended in 500 μl (5 μl was injected on column) of 75% solvent A (isopropyl alcohol/hexanes; 4:3; v/v) and 25% solvent B (isopropyl alcohol/hexanes/water; 4:3:0.7; v/v/v containing 5 mM ammonium acetate). Samples were analyzed by LC coupled to tandem MS (LC/MS/MS).

Liquid chromatography/MS

Analysis was performed as described previously (18) with modifications. For normal phase separation, samples were injected onto an Ascentis-Si HPLC column (150 × 2.1 mm, 5 μm; Supelco) at a flow rate of 0.2 ml/min with 25% solvent B and 75% solvent A. Solvent B was maintained at 25% for 5 min and increased to 60% over 10 min and then to 95% over 5 min. The system was held at 95% solvent B for 20 min before re-equilibration at 25% for 14 min. Phospholipids were measured using an API4000 triple quadrupole mass spectrometer (AB Sciex). Positive ion mode was used to detect PC and phosphatidylethanolamine (PE) lipids with quadrupole 1 scanning an m/z range from 250 to 900 in 0.1-Da increments over 3 s. Negative ion mode was used to detect CL, phosphatidic acid (PA), phosphatidylinositol (PI), phosphatidylglycerol (PG), and phosphatidylserine (PS) with quadrupole 1 scanning an m/z range from 150 to 1600 in 0.1-Da increments over 4 s. Quantitation of the peak area was performed using AB Sciex MultiQuant software. Internal standards were used to validate retention times for each phospholipid class. Based on elution relative to the internal standard, phospholipids were converted from mass-to-charge to total number of acyl carbons and double bonds.

Statistics

All graphs were created and statistics were performed with GraphPad Prism version 7.0 software. Data are expressed as the mean ± S.D. of sample size n. Each n represents an individual mouse. Comparisons between control and $Acsl1^{M-/-}$ mice were performed by unpaired, two-tailed Student's t test. For the wire hang grip test, a nonparametric Mann–Whitney U test was performed. For central nuclei data and homogenate and mitochondrial ACSL activity, two-way analysis of variance was conducted. For multiple comparisons, multiple t tests were performed and corrected by the Holm–Sidak method. A p value of less than 0.05 was considered significant.

Author contributions—L. Z., F. P., G. I. S., and R. A. C. conceptualization; L. Z., F. P., S. A. M., G. I. S., and R. A. C. formal analysis; L. Z., F. P., L. B., A. L. S., P. A. Y., L. O. L., S. A. M., J.-P. C., R. J. P., and G. I. S. investigation; L. Z., L. B., L. O. L., S. A. M., J.-P. C., R. J. P., and G. I. S. methodology; L. Z. writing-original draft; L. Z., F. P., A. L. S., P. A. Y., L. O. L., E. L. K., and R. A. C. writing-review and editing; E. L. K. data curation; R. A. C. resources; R. A. C. supervision; R. A. C. funding acquisition; R. A. C. project administration.

References

1. Hue, L., and Taegtmeyer, H. (2009) The Randle cycle revisited: a new head for an old hat. *Am. J. Physiol. Endocrinol. Metab.* **297,** E578–E591 CrossRef Medline
2. Arany, Z. (2008) PGC-1 coactivators and skeletal muscle adaptations in health and disease. *Curr. Opin. Genet. Dev.* **18,** 426–434 CrossRef Medline
3. Argilés, J. M., Campos, N., Lopez-Pedrosa, J. M., Rueda, R., and Rodriguez-Mañas, L. (2016) Skeletal muscle regulates metabolism via interorgan crosstalk: roles in health and disease. *J. Am. Med. Dir. Assoc.* **17,** 789–796 CrossRef Medline
4. Kiens, B. (2006) Skeletal muscle lipid metabolism in exercise and insulin resistance. *Physiol. Rev.* **86,** 205–243 CrossRef Medline
5. Rinaldo, P., Matern, D., and Bennett, M. J. (2002) Fatty acid oxidation disorders. *Annu. Rev. Physiol.* **64,** 477–502 CrossRef Medline
6. Fukao, T., Watanabe, H., Orii, K., Takahashi, Y., Hirano, A., Kondo, T., Yamaguchi, S., Aoyama, T., and Kondo, N. (2001) Myopathic form of very-long chain acyl-CoA dehydrogenase deficiency: evidence for temperature-sensitive mild mutations in both mutant alleles in a Japanese girl. *Pediatr. Res.* **49,** 227–231 CrossRef Medline
7. Spiekerkoetter, U., Tokunaga, C., Wendel, U., Mayatepek, E., Exil, V., Duran, M., Wijburg, F. A., Wanders, R. J., and Strauss, A. W. (2004) Changes in blood carnitine and acylcarnitine profiles of very long-chain acyl-CoA dehydrogenase-deficient mice subjected to stress. *Eur J. Clin. Invest.* **34,** 191–196 CrossRef Medline
8. Corti, S., Bordoni, A., Ronchi, D., Musumeci, O., Aguennouz, M., Toscano, A., Lamperti, C., Bresolin, N., and Comi, G. P. (2008) Clinical features and new molecular findings in carnitine palmitoyltransferase II (CPT II) deficiency. *J. Neurol. Sci.* **266,** 97–103 CrossRef Medline
9. DiMauro, S., and DiMauro, P. M. (1973) Muscle carnitine palmityltransferase deficiency and myoglobinuria. *Science* **182,** 929–931 CrossRef Medline
10. Schatz, U. A., and Ensenauer, R. (2010) The clinical manifestation of MCAD deficiency: challenges towards adulthood in the screened population. *J. Inherit. Metab. Dis.* **33,** 513–520 CrossRef Medline
11. Watt, M. J., and Hoy, A. J. (2012) Lipid metabolism in skeletal muscle: generation of adaptive and maladaptive intracellular signals for cellular function. *Am. J. Physiol. Endocrinol. Metab.* **302,** E1315–E1328 CrossRef Medline
12. Watkins, P. A., Maiguel, D., Jia, Z., and Pevsner, J. (2007) Evidence for 26 distinct acyl-coenzyme A synthetase genes in the human genome. *J. Lipid Res.* **48,** 2736–2750 CrossRef Medline
13. Schuler, A. M., and Wood, P. A. (2002) Mouse models for disorders of mitochondrial fatty acid β-oxidation. *ILAR J.* **43,** 57–65 CrossRef Medline
14. Ellis, J. M., Li, L. O., Wu, P. C., Koves, T. R., Ilkayeva, O., Stevens, R. D., Watkins, S. M., Muoio, D. M., and Coleman, R. A. (2010) Adipose acyl-CoA synthetase-1 directs fatty acids toward beta-oxidation and is required for cold thermogenesis. *Cell Metab.* **12,** 53–64 CrossRef Medline
15. Ellis, J. M., Mentock, S. M., Depetrillo, M. A., Koves, T. R., Sen, S., Watkins, S. M., Muoio, D. M., Cline, G. W., Taegtmeyer, H., Shulman, G. I., Willis, M. S., and Coleman, R. A. (2011) Mouse cardiac acyl coenzyme a synthetase 1 deficiency impairs fatty acid oxidation and induces cardiac hypertrophy. *Mol. Cell Biol.* **31,** 1252–1262 CrossRef Medline
16. Li, L. O., Grevengoed, T. J., Paul, D. S., Ilkayeva, O., Koves, T. R., Pascual, F., Newgard, C. B., Muoio, D. M., and Coleman, R. A. (2015) Compartmentalized acyl-CoA metabolism in skeletal muscle regulates systemic glucose homeostasis. *Diabetes* **64,** 23–35 CrossRef Medline
17. Grevengoed, T. J., Martin, S. A., Katunga, L., Cooper, D. E., Anderson, E. J., Murphy, R. C., and Coleman, R. A. (2015) Acyl-CoA synthetase 1 deficiency alters cardiolipin species and impairs mitochondrial function. *J. Lipid Res.* **56,** 1572–1582 CrossRef Medline
18. Grevengoed, T. J., Cooper, D. E., Young, P. A., Ellis, J. M., and Coleman, R. A. (2015) Loss of long-chain acyl-CoA synthetase isoform 1 impairs cardiac autophagy and mitochondrial structure through mechanistic target of rapamycin complex 1 activation. *FASEB J.* **29,** 4641–4653 CrossRef Medline

19. Smith, O. L., and Davidson, S. B. (1982) Shivering thermogenesis and glucose uptake by muscles of normal or diabetic rats. *Am. J. Physiol.* **242,** R109–R115 CrossRef Medline
20. Hargreaves, M. (2000) Skeletal muscle metabolism during exercise in humans. *Clin. Exp. Pharmacol. Physiol.* **27,** 225–228 CrossRef Medline
21. Wicks, S. E., Vandanmagsar, B., Haynie, K. R., Fuller, S. E., Warfel, J. D., Stephens, J. M., Wang, M., Han, X., Zhang, J., Noland, R. C., and Mynatt, R. L. (2015) Impaired mitochondrial fat oxidation induces adaptive remodeling of muscle metabolism. *Proc. Natl. Acad. Sci. U.S.A.* **112,** E3300–E3309 CrossRef Medline
22. Mashek, D. G., Li, L. O., and Coleman, R. A. (2007) Long-chain acyl-CoA synthetases and fatty acid channeling. *Future Lipidol.* **2,** 465–476 CrossRef Medline
23. Tedesco, F. S., Dellavalle, A., Diaz-Manera, J., Messina, G., and Cossu, G. (2010) Repairing skeletal muscle: regenerative potential of skeletal muscle stem cells. *J. Clin. Invest.* **120,** 11–19 CrossRef Medline
24. Vissing, J. (2016) Exercise training in metabolic myopathies. *Rev. Neurol.* (*Paris*) **172,** 559–565 CrossRef Medline
25. Chargé, S. B., and Rudnicki, M. A. (2004) Cellular and molecular regulation of muscle regeneration. *Physiol. Rev.* **84,** 209–238 CrossRef Medline
26. Sandri, M., El Meslemani, A. H., Sandri, C., Schjerling, P., Vissing, K., Andersen, J. L., Rossini, K., Carraro, U., and Angelini, C. (2001) Caspase 3 expression correlates with skeletal muscle apoptosis in Duchenne and facioscapulo human muscular dystrophy: a potential target for pharmacological treatment? *J. Neuropathol. Exp. Neurol.* **60,** 302–312 CrossRef Medline
27. Porter, A. G., and Jänicke, R. U. (1999) Emerging roles of caspase-3 in apoptosis. *Cell Death Differ.* **6,** 99–104 CrossRef Medline
28. Ruest, L. B., Khalyfa, A., and Wang, E. (2002) Development-dependent disappearance of caspase-3 in skeletal muscle is post-transcriptionally regulated. *J. Cell Biochem.* **86,** 21–28 CrossRef Medline
29. Chen, H., Vermulst, M., Wang, Y. E., Chomyn, A., Prolla, T. A., McCaffery, J. M., and Chan, D. C. (2010) Mitochondrial fusion is required for mtDNA stability in skeletal muscle and tolerance of mtDNA mutations. *Cell* **141,** 280–289 CrossRef Medline
30. He, J., Watkins, S., and Kelley, D. E. (2001) Skeletal muscle lipid content and oxidative enzyme activity in relation to muscle fiber type in type 2 diabetes and obesity. *Diabetes* **50,** 817–823 CrossRef Medline
31. Handschin, C., Chin, S., Li, P., Liu, F., Maratos-Flier, E., Lebrasseur, N. K., Yan, Z., and Spiegelman, B. M. (2007) Skeletal muscle fiber-type switching, exercise intolerance, and myopathy in PGC-1α muscle-specific knock-out animals. *J. Biol. Chem.* **282,** 30014–30021 CrossRef Medline
32. Hancock, C. R., Han, D. H., Chen, M., Terada, S., Yasuda, T., Wright, D. C., and Holloszy, J. O. (2008) High-fat diets cause insulin resistance despite an increase in muscle mitochondria. *Proc. Natl. Acad. Sci. U.S.A.* **105,** 7815–7820 CrossRef Medline
33. Frezza, C., Cipolat, S., and Scorrano, L. (2007) Measuring mitochondrial shape changes and their consequences on mitochondrial involvement during apoptosis. *Methods Mol. Biol.* **372,** 405–420 CrossRef Medline
34. Heden, T. D., Neufer, P. D., and Funai, K. (2016) Looking beyond structure: membrane phospholipids of skeletal muscle mitochondria. *Trends Endocrinol. Metab.* **27,** 553–562 CrossRef Medline
35. Vergeade, A., Bertram, C. C., Bikineyeva, A. T., Zackert, W. E., Zinkel, S. S., May, J. M., Dikalov, S. I., Roberts, L. J., 2nd, and Boutaud, O. (2016) Cardiolipin fatty acid remodeling regulates mitochondrial function by modifying the electron entry point in the respiratory chain. *Mitochondrion* **28,** 88–95 CrossRef Medline
36. Radley-Crabb, H. G., Marini, J. C., Sosa, H. A., Castillo, L. I., Grounds, M. D., and Fiorotto, M. L. (2014) Dystropathology increases energy expenditure and protein turnover in the mdx mouse model of duchenne muscular dystrophy. *PLoS One* **9,** e89277 CrossRef Medline
37. MacLennan, P. A., and Edwards, R. H. (1990) Protein turnover is elevated in muscle of mdx mice in vivo. *Biochem. J.* **268,** 795–797 CrossRef Medline
38. Hauerslev, S., Sveen, M. L., Vissing, J., and Krag, T. O. (2013) Protein turnover and cellular stress in mildly and severely affected muscles from patients with limb girdle muscular dystrophy type 2I. *PLoS One* **8,** e66929 CrossRef Medline
39. Goodman, C. A., and Hornberger, T. A. (2013) Measuring protein synthesis with SUnSET: a valid alternative to traditional techniques? *Exerc. Sport Sci. Rev.* **41,** 107–115 CrossRef Medline
40. Rennie, M. J., and Tipton, K. D. (2000) Protein and amino acid metabolism during and after exercise and the effects of nutrition. *Annu. Rev. Nutr.* **20,** 457–483 CrossRef Medline
41. Harber, M. P., Konopka, A. R., Jemiolo, B., Trappe, S. W., Trappe, T. A., and Reidy, P. T. (2010) Muscle protein synthesis and gene expression during recovery from aerobic exercise in the fasted and fed states. *Am. J. Physiol. Regul. Integr. Comp. Physiol.* **299,** R1254–R1262 CrossRef Medline
42. Atherton, P. J., and Smith, K. (2012) Muscle protein synthesis in response to nutrition and exercise. *J. Physiol.* **590,** 1049–1057 CrossRef Medline
43. Grevengoed, T. J., Klett, E. L., and Coleman, R. A. (2014) Acyl-CoA metabolism and partitioning. *Annu. Rev. Nutr.* **34,** 1–30 CrossRef Medline
44. Pascual, F., and Coleman, R. A. (2016) Fuel availability and fate in cardiac metabolism: A tale of two substrates. *Biochim. Biophys. Acta* **1861,** 1425–1433 CrossRef Medline
45. Weber-Carstens, S., Schneider, J., Wollersheim, T., Assmann, A., Bierbrauer, J., Marg, A., Al Hasani, H., Chadt, A., Wenzel, K., Koch, S., Fielitz, J., Kleber, C., Faust, K., Mai, K., Spies, C. D., *et al.* (2013) Critical illness myopathy and GLUT4: significance of insulin and muscle contraction. *Am. J. Respir. Crit. Care Med.* **187,** 387–396 CrossRef Medline
46. Bujak, A. L., Crane, J. D., Lally, J. S., Ford, R. J., Kang, S. J., Rebalka, I. A., Green, A. E., Kemp, B. E., Hawke, T. J., Schertzer, J. D., and Steinberg, G. R. (2015) AMPK activation of muscle autophagy prevents fasting-induced hypoglycemia and myopathy during aging. *Cell Metab.* **21,** 883–890 CrossRef Medline
47. Wagenmakers, A. J. (1998) Muscle amino acid metabolism at rest and during exercise: role in human physiology and metabolism. *Exerc. Sport Sci. Rev.* **26,** 287–314 Medline
48. Shimomura, Y., Murakami, T., Nakai, N., Nagasaki, M., and Harris, R. A. (2004) Exercise promotes BCAA catabolism: effects of BCAA supplementation on skeletal muscle during exercise. *J. Nutr.* **134,** 1583S–1587S CrossRef Medline
49. Shimomura, Y., Yamamoto, Y., Bajotto, G., Sato, J., Murakami, T., Shimomura, N., Kobayashi, H., and Mawatari, K. (2006) Nutraceutical effects of branched-chain amino acids on skeletal muscle. *J. Nutr.* **136,** 529S–532S CrossRef Medline
50. MacLean, D. A., Graham, T. E., and Saltin, B. (1994) Branched-chain amino acids augment ammonia metabolism while attenuating protein breakdown during exercise. *Am. J. Physiol.* **267,** E1010–E1022 CrossRef Medline
51. Shadrach, J. L., and Wagers, A. J. (2011) Stem cells for skeletal muscle repair. *Philos. Trans. R. Soc. Lond. B Biol. Sci.* **366,** 2297–2306 CrossRef Medline
52. Tidball, J. G. (2011) Mechanisms of muscle injury, repair, and regeneration. *Compr. Physiol.* **1,** 2029–2062 CrossRef Medline
53. Tucci, S., Pearson, S., Herebian, D., and Spiekerkoetter, U. (2013) Long-term dietary effects on substrate selection and muscle fiber type in very-long-chain acyl-CoA dehydrogenase deficient (VLCAD(−/−)) mice. *Biochim. Biophys. Acta* **1832,** 509–516 CrossRef Medline
54. Tucci, S., Mingirulli, N., Wehbe, Z., Dumit, V. I., Kirschner, J., and Spiekerkoetter, U. (2018) Mitochondrial fatty acid biosynthesis and muscle fiber plasticity in very long-chain acyl-CoA dehydrogenase-deficient mice. *FEBS Lett.* **592,** 219–232 CrossRef Medline
55. Rocchi, A., Milioto, C., Parodi, S., Armirotti, A., Borgia, D., Pellegrini, M., Urciuolo, A., Molon, S., Morbidoni, V., Marabita, M., Romanello, V., Gatto, P., Blaauw, B., Bonaldo, P., Sambataro, F., *et al.* (2016) Glycolytic-to-oxidative fiber-type switch and mTOR signaling activation are early-onset features of SBMA muscle modified by high-fat diet. *Acta Neuropathol.* **132,** 127–144 CrossRef Medline
56. Webster, C., Silberstein, L., Hays, A. P., and Blau, H. M. (1988) Fast muscle fibers are preferentially affected in Duchenne muscular dystrophy. *Cell* **52,** 503–513 CrossRef Medline
57. Moens, P., Baatsen, P. H., and Maréchal, G. (1993) Increased susceptibility of EDL muscles from mdx mice to damage induced by contractions with stretch. *J. Muscle Res. Cell Motil.* **14,** 446–451 CrossRef Medline

58. Komiya, Y., Sawano, S., Mashima, D., Ichitsubo, R., Nakamura, M., Tatsumi, R., Ikeuchi, Y., and Mizunoya, W. (2017) Mouse soleus (slow) muscle shows greater intramyocellular lipid droplet accumulation than EDL (fast) muscle: fiber type-specific analysis. *J. Muscle Res. Cell Motil.* **38,** 163–173 CrossRef Medline
59. Listenberger, L. L., Han, X., Lewis, S. E., Cases, S., Farese, R. V., Jr., Ory, D. S., and Schaffer, J. E. (2003) Triglyceride accumulation protects against fatty acid-induced lipotoxicity. *Proc. Natl. Acad. Sci. U.S.A.* **100,** 3077–3082 CrossRef Medline
60. Bosma, M. (2016) Lipid droplet dynamics in skeletal muscle. *Exp. Cell Res.* **340,** 180–186 CrossRef Medline
61. Yao, H., and Ye, J. (2008) Long chain acyl-CoA synthetase 3-mediated phosphatidylcholine synthesis is required for assembly of very low density lipoproteins in human hepatoma Huh7 cells. *J. Biol. Chem.* **283,** 849–854 CrossRef Medline
62. Padanad, M. S., Konstantinidou, G., Venkateswaran, N., Melegari, M., Rindhe, S., Mitsche, M., Yang, C., Batten, K., Huffman, K. E., Liu, J., Tang, X., Rodriguez-Canales, J., Kalhor, N., Shay, J. W., Minna, J. D., *et al.* (2016) Fatty acid oxidation mediated by acyl-CoA synthetase long chain 3 is required for mutant KRAS lung tumorigenesis. *Cell Rep.* **16,** 1614–1628 CrossRef Medline
63. Li, L. O., Ellis, J. M., Paich, H. A., Wang, S., Gong, N., Altshuller, G., Thresher, R. J., Koves, T. R., Watkins, S. M., Muoio, D. M., Cline, G. W., Shulman, G. I., and Coleman, R. A. (2009) Liver-specific loss of long chain acyl-CoA synthetase-1 decreases triacylglycerol synthesis and β-oxidation and alters phospholipid fatty acid composition. *J. Biol. Chem.* **284,** 27816–27826 CrossRef Medline
64. Kelly, S. A., Zhao, L., Jung, K. C., Hua, K., Threadgill, D. W., Kim, Y., de Villena, F. P., and Pomp, D. (2017) Prevention of tumorigenesis in mice by exercise is dependent on strain background and timing relative to carcinogen exposure. *Sci. Rep.* **7,** 43086 CrossRef Medline
65. Kalueff, A. V., Fox, M. A., Gallagher, P. S., and Murphy, D. L. (2007) Hypolocomotion, anxiety and serotonin syndrome-like behavior contribute to the complex phenotype of serotonin transporter knockout mice. *Genes Brain Behav.* **6,** 389–400 CrossRef Medline
66. Ayala, J. E., Samuel, V. T., Morton, G. J., Obici, S., Croniger, C. M., Shulman, G. I., Wasserman, D. H., McGuinness, and NIH Mouse Metabolic Phenotyping Center Consortium (2010) Standard operating procedures for describing and performing metabolic tests of glucose homeostasis in mice. *Dis. Model. Mech.* **3,** 525–534 CrossRef Medline
67. Folch, J., Lees, M., and Sloane Stanley, G. H. (1957) A simple method for the isolation and purification of total lipides from animal tissues. *J. Biol. Chem.* **226,** 497–509 Medline
68. Bligh, E. G., and Dyer, W. J. (1959) A rapid method of total lipid extraction and purification. *Can. J. Biochem. Physiol.* **37,** 911–917 CrossRef Medline